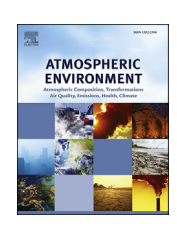
FISEVIER

Contents lists available at ScienceDirect

Atmospheric Environment

journal homepage: www.elsevier.com/locate/atmosenv



Impact of global climate change on ozone, particulate matter, and secondary organic aerosol concentrations in California: A model perturbation analysis



Jeremy R. Horne, Donald Dabdub

Computational Environmental Sciences Laboratory, Department of Mechanical & Aerospace Engineering, University of California, Irvine, Irvine, CA, 92697-3975, USA

HIGHLIGHTS

- Temperature increases dominate the impact on ozone, PM and SOA in all scenarios.
- Impact of increasing temperature is greatest in the northeast portion of the basin.
- The largest changes in ozone, PM, and SOA occur in areas with poor air quality.
- Air quality management strategies must consider chemistry-climate interactions.
- SOA concentrations are projected to decrease by over 15% due to climate change.

ARTICLE INFO

Article history:
Received 22 August 2016
Received in revised form
23 November 2016
Accepted 27 December 2016
Available online 28 December 2016

Keywords:
Air quality modeling
Ozone
Particulate matter
Secondary organic aerosols
South Coast Air Basin of California
Climate change

ABSTRACT

Air quality simulations are performed to determine the impact of changes in future climate and emissions on regional air quality in the South Coast Air Basin (SoCAB) of California. The perturbation parameters considered in this study include (1) temperature, (2) absolute humidity, (3) biogenic VOC emissions due to temperature changes, and (4) boundary conditions. All parameters are first perturbed individually. In addition, the impact of simultaneously perturbing more than one parameter is analyzed. Air quality is simulated with meteorology representative of a summertime ozone pollution episode using both a baseline 2005 emissions inventory and a future emissions projection for the year 2023. Different locations within the modeling domain exhibit varying degrees of sensitivity to the perturbations considered. Afternoon domain wide average ozone concentrations are projected to increase by 13–18% as a result of changes in future climate and emissions. Afternoon increases at individual locations range from 10 to 36%. The change in afternoon particulate matter (PM) levels is a strong function of location in the basin, ranging from -7.1% to +4.7% when using 2005 emissions and -8.6% to +1.7% when using 2023 emissions. Afternoon secondary organic aerosol (SOA) concentrations for the entire domain are projected to decrease by over 15%, and the change in SOA levels is not a strong function of the emissions inventory utilized. Temperature increases play the dominant role in determining the overall impact on ozone, PM, and SOA concentrations in both the individual and combined perturbation scenarios.

© 2016 Elsevier Ltd. All rights reserved.

1. Introduction

The frequency and severity of air pollution episodes depends strongly on both emissions and meteorological conditions. The

E-mail addresses: jrhorne@uci.edu (J.R. Horne), ddabdub@uci.edu (D. Dabdub).

successful implementation of control strategies requires a detailed understanding of the chemistry-meteorology-climate interactions of both gas-phase and particulate pollutants. Traditional modeling studies estimate the effectiveness of potential emission control strategies by using recent meteorological conditions (Chock et al., 1999; Marr and Harley, 2002; Nguyen and Dabdub, 2002). However, model projections indicate significant changes to global and regional climate for both the near- (2020–2050) and long-term (2070–2099) (Snyder et al., 2002; Hayhoe et al., 2004; Coquard

^{*} Corresponding author. Department of Mechanical & Aerospace Engineering, The Henry Samueli School of Engineering, University of California, Irvine, Irvine, CA, 92697-3975. USA.

et al., 2004; Mahmud et al., 2010; Zhao et al., 2011b). The traditional modeling approach of using recent climate conditions may no longer be appropriate to estimate future air quality (Steiner et al., 2006). As 21st century climate change becomes an increasingly pressing issue, modeling studies must incorporate future climate scenarios to understand the implications of climate change on air quality. Modeling studies must also consider the potential impact of changes in both biogenic and anthropogenic emissions under future climate scenarios. Furthermore, in addition to gas-phase pollutants such as ozone, particulate matter (PM) and, more specifically, secondary organic aerosols (SOA), must be examined in detail to provide a comprehensive assessment of the impact of future climate and emission changes on air quality.

Ambient air quality standards exist at both the federal level and state level in California for ozone and particulates with aerodynamic diameters <10 μ m (PM₁₀) and <2.5 μ m (PM_{2.5}). However, despite having more stringent standards than those at the federal level for several criteria pollutants, Californians are exposed to daily concentrations of ozone among the highest in the nation (Ostro et al., 2006; Zhao et al., 2011a, 2011b). Additional modeling work in this area is needed because of the potential for adverse effects on public health from rising ozone and PM levels (Ebi and McGregor, 2008). Together, ozone and PM (particularly PM_{2.5}) are of most concern for human health (Tai et al., 2010; Perera and Sanford, 2011). Ozone, inorganic PM, and organic PM also affect light scattering and interact with terrestrial radiation, leading to climate forcing effects and contributing to poor visibility (Aw and Kleeman, 2003; Liao et al., 2006; Racherla and Adams, 2006; Jacob and Winner, 2009).

It is essential that air quality management strategies account for possible climate driven changes in pollutant levels. The potential air quality benefits of emission control policies and associated reductions in precursor emissions such as NO_X and volatile organic compounds (VOCs) may be offset by increasing temperatures or other climate change induced meteorological changes. For example, Kelly et al. (2012) showed that the projected impact of climate change alone (with no changes in emissions) is to cause a degradation of air quality for the years 2041–2050, with increases in both ozone and PM_{2.5} concentrations in North America. However, their results also suggested that simultaneous reductions in anthropogenic precursor emissions reduce or reverse worsening air quality due to climate change. Gao et al. (2013) showed that the impact of emission and climate change on projected ozone concentrations depends strongly on the representative concentration pathway (RCP) scenario used and that ozone change patterns show consistent seasonal variations. Their results indicated that by the end of the 2050s projected ozone concentrations decrease significantly for most of the continental United States under a lowmedium future emissions scenario (RCP 4.5), but decrease much less or even increase under a fossil-fuel intensive future emission scenario (RCP 8.5). The authors concluded that reducing methane emissions will greatly benefit future ozone control but reducing NO_X emissions could lead to ozone increases, particularly in highly populated urban areas and during winter, due to decreased NO titration effect. More recently, Val Martin et al. (2015) found that climate change alone lead to a significant increase in projected maximum daily 8-hr average ozone (MDA8) by 2050 over most of the United States. However, they also predicted that air quality will improve significantly across most of the U.S. if stringent domestic emissions controls are applied in the future. Similar to Gao et al. (2013), Val Martin et al. (2015) found that increased methane levels in the RCP 8.5 scenario cause ozone concentrations to increase in the central and western U.S. despite reductions in other anthropogenic precursor emissions. In early 2016, He et al. showed that the contribution of future climate change (2048–2052) to ozone concentrations is positive for most regions in the U.S. due primarily to increased ambient temperatures and biogenic emissions. However, when future emissions changes were considered simultaneously under the 'clean' A1B scenario, surface ozone concentrations were projected to decrease despite the positive contribution from climate change. The authors also found that lateral boundary conditions can influence future ozone projections with a magnitude similar to climate change alone, particularly in the western United States.

Several other studies have investigated the impact of the transpacific transport of air pollutants from Asia to North America. For example, Cooper et al. (2010) found that free tropospheric ozone increases due to rising Asian ozone precursor emissions can affect surface air quality, particularly in western North America. Their results agree with other studies who indicated that transport from Asian would cause increased springtime surface ozone concentrations in western North America despite decreasing domestic emissions. Lin et al. (2012) conducted a detailed analysis on the mechanisms and impacts of Asian pollution plumes transported into western U.S. surface air and showed that Asian pollution enhancements to daily maximum 8-hr ozone concentrations in surface air are about 2-5 ppb for southern California in May-June 2010, with larger increases at higher elevations. Furthermore, the authors estimated that for a 75 ppbv threshold, 53% of modeled MDA8 ozone exceedances for the southwestern USA would not have occurred in the absence of Asian anthropogenic emissions. More recently, Verstraeten et al. (2015) analyzed the impact of Chinese pollution on ozone concentrations in the western United States. They reported that the influence of Chinese pollution on the western U.S. is greatest during spring, and the contribution to freetropospheric ozone is greater than the contribution to near-surface ozone, consistent with previous studies. Overall, these studies showed that attainment of ambient air quality standards in the western U.S. may be hindered by increases in background ozone concentrations due to trans-pacific transport of ozone and its precursors from Asia, suggesting the need for global efforts to address regional air quality and climate change (Cooper et al., 2010; Lin et al., 2012; Verstraeten et al., 2015). However, the relatively coarse resolution used in large scale model simulations makes it difficult to discern meso-scale impacts in regions such as southern California, highlighting the need for high-resolution regional modeling studies.

Several modeling studies have examined the effect of climate change related perturbations on ozone and inorganic particulate air quality in California (Aw and Kleeman, 2003; Carreras-Sospedra et al., 2006; Steiner et al., 2006; Kleeman, 2008; Mahmud et al., 2008, 2010, 2012; Millstein and Harley, 2009). Other studies have focused on analyzing the impact of climate change on present and future simulated meteorological conditions in California (Zhao et al., 2011a, 2011b). An early study by Aw and Kleeman (2003) showed that temperature is the single most important meteorological variable influencing both gas-phase and particulate air quality in southern California due to its effect on chemical reaction rates and gas-to-particle partitioning. A later study by Steiner et al. (2006) examined the impact of changes in future climate and emissions on ozone air quality in California. Individual perturbations to temperature, atmospheric water vapor, and biogenic VOC emissions each caused a 1–5% increase in daily peak ozone levels. Simultaneous perturbations combining climate change effects performed by Steiner et al. (2006) resulted in ozone increases of 3–10%. Changes in chemical boundary conditions at the western inflow for ozone, CO, and methane caused ozone levels to increase by 6% in coastal areas, but by only 1–2% inland.

More recently, Millstein and Harley (2009) used perturbation scenarios similar to Steiner et al. (2006) to examine the effect of a

variety of future climate and emissions related perturbations on ozone air quality in southern California for a summertime high-ozone episode in 2005. They found increases in peak ozone levels across the domain as a result of increased temperatures. The combined climate forcing case described by Millstein and Harley (2009) caused increases in peak ozone across the domain ranging from 3 to 15 ppb (parts per billion). They concluded that additional controls on anthropogenic emissions will be needed to offset the impact of climate change on ozone air quality in southern California.

Other existing analyses utilize global models whose resolution is not sufficient to provide an accurate and consistent picture of the response of ozone, PM, and SOA to climate change in urban areas (Brasseur et al., 2006; Liao et al., 2006; Racherla and Adams, 2006; Heald et al., 2008; Lin et al., 2016). Although ozone production increases with increasing temperatures in polluted areas, several global studies report ozone decreases in remote areas due to the increased destruction of ozone by water vapor at these higher temperatures (Brasseur et al., 2006; Racherla and Adams, 2006; Millstein and Harley, 2009). Racherla and Adams (2006) simulated a future climate scenario for the year 2050 and showed that at the model surface layer, some regions show increases in the concentration of fine particulate matter species while others show decreases. Lin et al. (2016) used an Earth system model coupled with an explicit SOA formation module to estimate the impact of changes in climate, emissions, and land use on SOA concentrations at the global scale. They reported that although the global SOA burden is nearly constant from year 2000 to year 2100, regional SOA concentrations show large variations, with simulated decreases of 7% over the United States. Even in high-resolution modeling studies of local effects on air quality, the effects of climate change on ozone vary strongly by location across different air basins (Aw and Kleeman, 2003; Carreras-Sospedra et al., 2006; Steiner et al., 2006; Millstein and Harley, 2009).

While a few regional modeling studies have examined the impact of changes in future climate and emissions on inorganic and organic PM concentrations in California (Aw and Kleeman, 2003; Kleeman, 2008; Mahmud et al., 2010, 2012), the impact of climate change on SOA concentrations has been studied mostly on a global scale (Liao et al., 2006; Heald et al., 2008; Lin et al., 2016). This study is the first of its kind to analyze the impact of climate change on SOA concentrations at the regional scale in southern California. Overall, there is a large uncertainty regarding the dynamic response of both inorganic and organic PM, particularly SOA, to climate change induced meteorological changes such as increasing temperatures, increasing absolute humidity, and changes in relative humidity and biogenic emissions associated with an increase in temperature (Jacob and Winner, 2009). Sensitivity to climate change parameters varies greatly based on location, local emissions, chemical species of interest, time of day, as well as a host of other variables. The highly intertwined nature of variables such as temperature, humidity, and biogenic emissions further exacerbates the need for additional modeling studies to fill current knowledge gaps and confirm results from existing studies. The use of highresolution regional air quality models with highly developed aerosol modules is necessary to study these effects on local air quality in California. Furthermore, because the effects of climate change are highly spatially dependent, a fine-scale grid with detailed topography and is required. Temporal and spatial variations in the concentrations of atmospheric constituents is need to provide a detailed picture of the response of air quality to climate change in urban areas.

The purpose of the present study is to examine the effect of changes in future climate and emissions on regional air quality utilizing a three-dimensional air quality model. This paper is one of the first of its kind to examine these effects qualitatively and quantitatively for ozone, PM_{2.5}, PM₁₀, and SOA, as well as for specific PM components such as nitrates and sulfates. Changes in both the concentration and the distribution of key atmospheric pollutants are examined in detail. Results for ozone and PM25 are compared to existing studies, while results for SOA represent the key findings of this paper. Such results have not been reported in existing high-resolution regional modeling studies of California. Model runs are performed using both a base-case emissions inventory from 2005 and a projected future emissions inventory for the year 2023 documented in the 2007 Air Quality Management Plan (AQMP) developed by the South Coast Air Quality Management District (SCAQMD). The influence of changes in western inflow boundary conditions of ozone, NO, and NO₂ similar to those used by Steiner et al. (2006) are also considered. The modeling domain encompasses the South Coast Air Basin (SoCAB) of California, which contains a diverse landscape with many microclimates, urban and suburban areas, and a wide distribution of biogenic and anthropogenic emissions. This domain provides an ideal test bed to study the effects of climate change on air quality. Results will have far-reaching implications for other regions with similar geographic and meteorological conditions.

This work begins with a description of the UCI-CIT Airshed model and the specific future emissions and climate scenarios that are considered. The basis for, and specifics of, each perturbation scenario are discussed in detail in the Supplementary material and summarized in Table 1. Perturbations are considered individually as well as collectively to isolate the impact of each parameter and assess interactions among the variables. Results are presented in section 3 with subsections for each of ozone, PM and SOA. Section 4 summarizes key results and presents conclusions.

2. Methodology

The effects of climate change on air quality in southern California are studied by a model perturbation analysis with changes in one or more of the following parameters: temperature, absolute humidity, biogenic emissions, and boundary conditions. A complete list of all perturbation scenarios, a brief description, and the nomenclature utilized in this study is provided in Table 1. More detailed information regarding the basis for and specific of each perturbation scenario can be found in the Supplementary material. In order to determine the relative importance of each parameter, this paper examines the impact of changing individual parameters as well as combined effects that result from simultaneous perturbations to more than one parameter at a time. Furthermore, the influence of changes in future anthropogenic emissions is examined using projected emissions for the year 2023. Thus, each perturbation scenario is first performed using a 2005 emissions inventory and results are compared to the 2005 emissions base case where meteorological inputs are unchanged. Results for the perturbation scenarios performed when using 2023 emissions are compared to a 2023 emissions base case rather than to the 2005 emissions base case to isolate the effects of the perturbations.

2.1. Model description

The University of California, Irvine — California Institute of Technology (UCI-CIT) regional airshed model with a state-of-theart chemical mechanism and aerosol module is used here. The UCI-CIT model incorporates an expanded version of the Caltech atmospheric chemical mechanism (CACM, Griffin et al., 2002a,b; Griffin et al., 2005) and has been used to study the air quality of the SoCAB extensively (Nguyen and Dabdub, 2002; Jimenez et al., 2003; Carreras-Sospedra et al., 2006; Ensberg et al., 2010; Chang

 Table 1

 List of all perturbation scenarios considered in this study and corresponding nomenclature and description.

Perturbation Scenario	Nomenclature	Description
Low Temperature: $\Delta T = +1$ °C	LTEMP	Temperature values are increased uniformly by $+1$ °C while all other conditions remain unchanged from the base case. This temperature increase represents a near-term climate projection, i.e., years $2020-2050$.
High Temperature: $\Delta T = +3 {}^{\circ}C$	НТЕМР	Temperature values are increased uniformly by +3 °C while all other conditions remain unchanged from the base case. This temperature increase represents a long-term climate projection, i.e., years 2070–2099.
Absolute Humidity	HUMID	Absolute humidity and relative humidity both increase while all other conditions remain unchanged from the base case. Absolute humidity is increased such that relative humidity would be the same as in the base case when temperatures are increased by +3 °C, even though temperature values remain equal to the base case in this scenario.
Biogenic Emissions	BIO	Biogenic emissions of isoprene are increased based on a temperature increase of $+3$ °C while all other conditions (including temperature) remain equal to those of the base case.
High Temperature and Absolute Humidity	HTEMP + HUMID	Temperature values are increased uniformly by $+3$ °C and absolute humidity values are increased such that relative humidity remains the same as in the base case.
High Temperature and Biogenic Emissions	HTEMP + BIO	Temperature values are increased uniformly by $+3$ °C and biogenic emissions of isoprene are increased by approximately 60% based on this temperature increase.
High Temperature, Absolute Humidity and Biogenic Emissions	HTEMP + HUMID + BIO	Temperature values are increased uniformly by +3 °C and biogenic emissions and absolute humidity are both increased in accordance with this temperature increase. Relative humidity remains the same as the base case.
Inflow Boundary Conditions	ВС	Western boundary conditions of O_3 , NO, and NO_2 are increased from 40 ppb to 55 ppb, 0.3 ppb -1 ppb, and 0.5 ppb -1 ppb, respectively. Boundary conditions along the northern, southern, and eastern edges of the domain remain unchanged from base case levels.
High Temperature, Absolute Humidity, Bioger Emissions and Inflow Boundary Conditions		BC Temperature values are increased uniformly by +3 °C and biogenic emissions and absolute humidity are both increased in accordance with this temperature increase. Relative humidity remains the same as the base case. Inflow boundary conditions are changed as described in the BC scenario.

et al., 2010; Carreras-Sospedra et al., 2010; Cohan et al., 2013; Dawson et al., 2016). The three dimensional model contains a total of 476 reactions and 174 species. Of these, 37 are aerosol phase species, each of which is sorted into eight size bins. The UCI-CIT model utilizes a fully coupled hydrophilic-hydrophobic model for predicting secondary organic aerosol formation (Griffin et al., 2002a,b; Griffin et al., 2003; Griffin et al., 2005). Several studies have used the UCI-CIT model to investigate secondary organic aerosol formation, dynamics, reactivity, and partitioning phase preference in the SoCAB (Griffin et al., 2002b; Carreras-Sospedra et al., 2005; Vutukuru et al., 2006; Chang et al., 2010; Cohan et al., 2013). For a more detailed description of recent updates made to the UCI-CIT model and its chemical mechanism and SOA modules, the reader is referred to Dawson et al. (2016). The irregular shaped model domain contains 994 fixed-grid computational cells with 5 km \times 5 km horizontal resolution and encompasses the SoCAB, extending west to Simi Valley and east to Palm Springs. The domain extends as far south as Laguna Beach and north to Hesperia, as shown in Fig. 1. The SoCAB provides a unique setting to study the dynamic response of ozone, SOA, and primary organic and inorganic particulate matter to climate change as it contains coastal regions, urban and suburban areas, and low desert inland areas with the San Gabriel and San Bernardino Mountains acting as a barrier to the transport of pollutants further inland from sea breeze effects.

2.2. Emissions

Air quality is simulated over the three-day period August 27-29 with meteorology representative of a summertime ozone pollution episode using both a baseline 2005 emissions inventory and a future emissions projection for the year 2023 that includes significant NO_X and VOC controls to achieve attainment of ozone standards. Both the 2005 and the 2023 emissions inventories are documented in the 2007 AQMP formulated by the SCAQMD. The Final 2007 AQMP is designed to meet both federal and state Clear Air Act requirements for all areas under the jurisdiction of the SCAQMD, which includes the SoCAB (SCAQMD, 2007). The baseline

2023 emissions projection is based primarily on reductions in VOC, NO_X, PM_{2.5}, and CO emissions from both mobile and stationary sources (SCAQMD, 2007). In addition to baseline emissions projections, the SCAQMD provides another emissions projection for the year 2023 known as the "controlled" case. The 2023 controlled case utilized here features additional reductions in NO_X and VOC emissions compared with the baseline 2023 emissions projection to reach attainment of federal and state standards for ozone. Table S1 of the supplementary material shows total domain-wide anthropogenic emissions of key precursor species in both the 2005 and controlled 2023 emissions inventories. Total emissions of NO, NO₂, and SO₂ are a factor of 3-4 lower in the controlled 2023 emissions case compared with the 2005 emissions case, while emissions of NH3 remain relatively unchanged. Formaldehyde (HCHO) and carbon monoxide (CO) emissions are about a factor of two lower in the controlled 2023 emissions case compared with the 2005 emissions case. Additional details on base and future year emissions inventories are described in appendix III of the 2007 AQMP (SCAQMD, 2007). The controlled 2023 emissions inventory used in this study also includes reductions in the background concentration of peroxyacetyl nitrate (PAN) based on analysis of long term trends in southern California conducted by Grosjean (2003) and Pollack et al. (2013). All references to emissions for the year 2023 hereafter refer to the controlled 2023 emissions inventory described above. Lastly, results from the first day of simulation are not considered so that perturbations to climate parameters and changes in emissions have sufficient time to drive changes in air quality and the influence of initial conditions is diminished.

3. Results and discussion

3.1. Ozone

3.1.1. Impact of temperature

The overall effect of each perturbation scenario on ozone air quality using 2023 emissions is shown in Table 2. The effect of increasing temperatures in the LTEMP and HTEMP scenarios is to

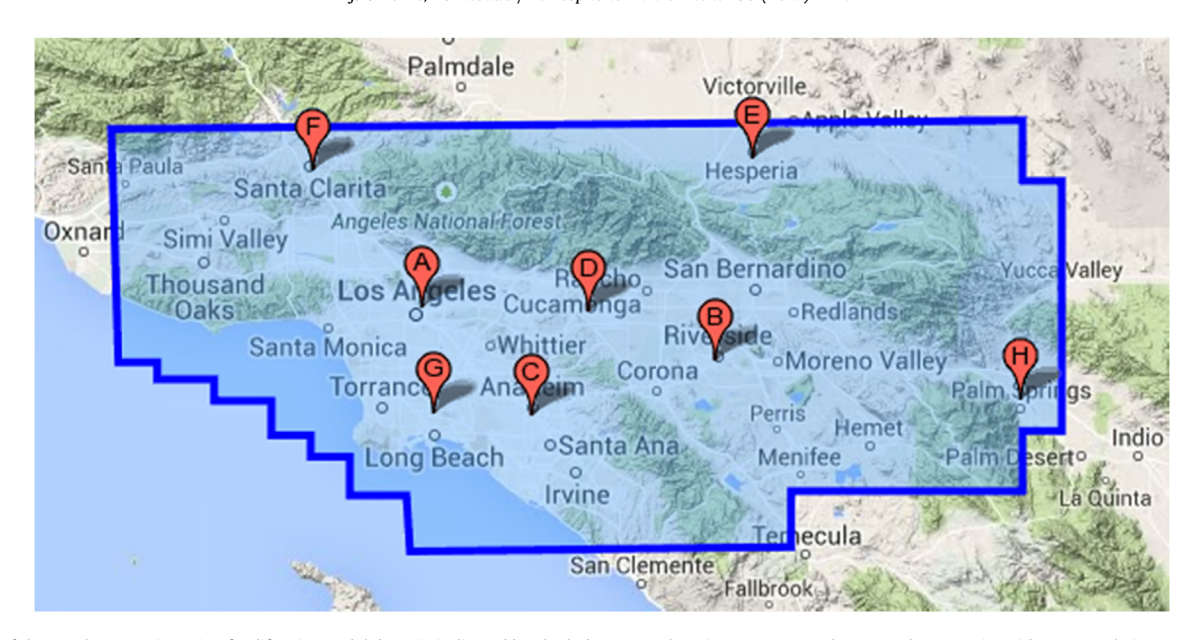


Fig. 1. Map of the South Coast Air Basin of California. Model domain indicated by shaded area. Key locations: A — Central Los Angeles; B — Riverside; C — Anaheim; D — Pomona; E — Hesperia; F — Newhall; G — North Long Beach; H — Palm Springs. Map data ©2014 Google, INEGI.

Table 2Domain wide averages at 16:00 h LT using 2023 emissions. Base case levels shown in top row. Difference and percent difference in concentration between the specified perturbation scenario and the base case shown in bottom rows. Positive values represent increases in concentration with respect to the base case. The dash (–) indicates that the difference is less than the number of significant figures shown (i.e., less than 0.1 change from base case levels).

Base Case	O ₃ (ppb)	$PM_{10} (\mu g/m^3)$	$PM_{2.5} (\mu g/m^3)$	SOA (μg/m ³)
	71	40	29	3.5
LTEMP	1.8, 2.6%	-0.5, -1.3%	-0.5, -1.7%	-0.2, -6.6%
HTEMP	5.5, 7.8%	-1.5, -3.9%	-1.4, -5.0%	-0.7, -19.7%
HUMID	-0.1, -0.1%	0.3, 0.6%	0.2, 0.8%	0.1, 2.0%
BIO	0.3, 0.4%	=	=	_
HTEMP + HUMID	5.5, 7.7%	-1.3, -3.3%	-1.2, -4.2%	-0.6, -18.1%
HTEMP + BIO	5.9, 8.3%	-1.6, -3.9%	-1.4, -5.0%	-0.7, -19.2%
HTEMP + HUMID + BIO	5.9, 8.2%	-1.4, -3.4%	-1.2, -4.3%	-0.6, -17.6%
BC	3.6, 5.0%	0.2, 0.6%	0.2, 0.6%	_
HTEMP + HUMID + BIO + BC	9.6, 13.5%	-1.2, -2.9%	-1.1, -3.8%	-0.6,-17.0%

increase ozone concentrations throughout the domain. When temperatures are increased by 3 °C, afternoon domain wide average ozone concentrations increase by 5.5 ppb, a 7.8% increase compared to the base case. In addition to affecting chemical reaction rates in the model, high temperatures favor the decomposition of PAN, increasing NO $_{\rm X}$ (Carreras-Sospedra et al., 2006). In brief, temperature has a significant effect on the formation of ozone in the SoCAB.

Looking at key individual locations within the domain, ozone concentrations consistently exhibit a positive response to temperature increases. The effect of each perturbation scenario on peak afternoon ozone concentrations at various locations within the SoCAB when using 2023 emissions is shown in Table 3. While the magnitude of the increase (in ppb) varies as a function of location within the basin, the *percentage* increase for most locations is about 10% in the HTEMP scenario when using 2023 emissions. Increases in ozone for the HTEMP scenario are roughly three times those seen in the LTEMP scenario for specific locations as well as on a domain wide average basis.

Changes in 24-h average ozone concentrations for the HTEMP scenario are shown in Fig. 2a for the 2023 emissions case. Contours reveal that the magnitude of the increase in ozone concentrations grows as one moves inland. Increasing temperatures causes little to no change in ozone levels for areas located along the coast. In terms of the meteorology and geography of the SoCAB, the presence of a

sea breeze results in a prevailing wind direction of north-northeast while the San Gabriel Mountain Range, located along the northeastern edge of the domain, acts as a barrier to transport of pollutants further inland. Overall, both afternoon and 24-h average ozone increases that result from the temperature perturbation scenarios are in line with existing modeling studies (Steiner et al., 2006; Kleeman, 2008; Millstein and Harley, 2009). Ozone increases due to increased temperatures are greatest in polluted areas with high anthropogenic emissions, while ozone concentrations in remote and coastal areas are generally less impacted by temperature perturbations.

3.1.2. Impact of humidity

Ozone concentrations are less sensitive to increases in the concentration of water vapor than to increases in temperature. In the HUMID scenario, increasing both relative and absolute humidity causes ozone increases in some areas but decreases in others. As a result, there is essentially no change in afternoon domain wide average ozone concentrations when using 2023 emissions (see Table 2). Table 3 reveals the extent to which changes in humidity impact ozone as a function of location in the basin. Long Beach experiences slight decreases in afternoon ozone because it is located near the coast and upwind of most anthropogenic emission sources. The greatest increases in 24-h average

Table 3Ozone concentration (ppb) for select locations at 16:00 h LT using 2023 emissions: Base case levels shown in top row. Difference and percent difference in ozone concentration between the specified perturbation scenario and the base case shown in bottom rows. Positive values represent increases in concentration with respect to the base case. The dash (–) indicates that the difference is less than the number of significant figures shown (i.e., less than 0.1 change from base case levels).

Base Case O ₃	Los Angeles	Riverside	Anaheim	Pomona	Newhall	Long Beach
	45	82	57	83	87	37
LTEMP	1.5, 3.4%	2.4, 2.9%	1.7, 3.1%	3.0, 3.6%	3.0, 3.5%	0.9, 2.5%
HTEMP	4.9, 10.7%	7.2, 8.8%	5.6, 9.9%	9.0, 10.9%	9.3, 10.7%	3.1, 8.2%
HUMID	0.4, 0.9%	-0.6, 0.8%	-1.0, -1.7%	4.5, 5.5%	-0.8, -0.9%	-0.1, -0.3%
BIO	0.1, 0.2%	0.3, 0.3%	-	1.6, 1.9%	-	0.1, 0.3%
HTEMP + HUMID	5.1, 11.4%	6.7, 8.1%	4.8, 8.4%	14.1, 17.1%	8.6, 9.9%	2.8, 7.5%
HTEMP + BIO	4.9, 10.9%	7.6, 9.3%	5.7, 10.0%	10.7, 13.0%	9.4, 10.8%	3.2, 8.5%
HTEMP + HUMID + BIO	5.2, 11.6%	7.0, 8.5%	4.7, 8.3%	15.6, 18.9%	8.8, 10.1%	2.9, 7.8%
BC	4.1, 9.0%	1.0, 1.2%	8.9, 15.6%	2.2, 2.6%	10.3, 11.9%	6.7, 17.8%
HTEMP + HUMID + BIO + BC	9.8, 21.7%	8.0, 9.7%	14.4, 25.4%	18.0, 21.9%	20.1, 23.1%	10.0, 26.8%

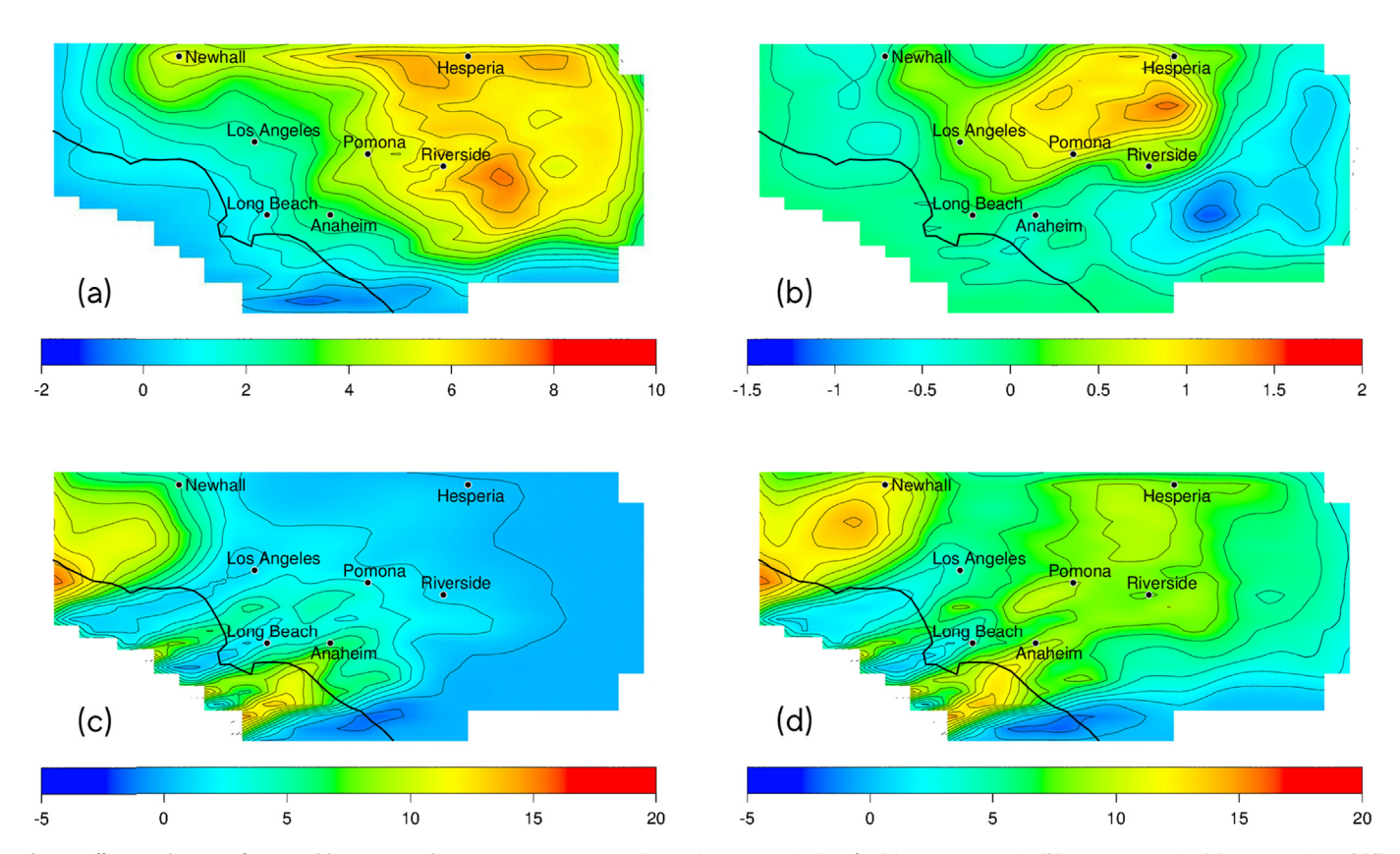


Fig. 2. Differences between future and base case 24-h average ozone concentrations using 2023 emissions for (a) HTEMP scenario, (b) HUMID scenario, (c) BC scenario, and (d) HTEMP + HUMID + BIO + BC scenario. Positive values represent increases in concentration with respect to the base case.

ozone levels occur east of Los Angeles, particularly north of Riverside (Fig. 2b). Ozone precursors such as NO_X and VOCs are affected by increases in water vapor concentrations due to increased production of HO_X from ozone photolysis (Jacob and Winner, 2009; Millstein and Harley, 2009). As a result, a decrease in NO_X levels causes ozone concentrations to increase in regions that are NO_X saturated and decrease in NO_X limited regions. Overall, results for the HUMID scenario are in agreement with existing studies that find that the sensitivity of ozone to humidity perturbations in polluted regions is weak and of variable sign (Dawson et al., 2007a; Jacob and Winner, 2009).

3.1.3. Impact of biogenic emissions

In the BIO perturbation scenario, the overall impact on ozone concentrations for the domain as a whole is small due to the spatial

distribution of isoprene emissions (Table 2). Similarly, all locations examined in Table 3 except for Pomona experience increases in afternoon ozone of less than 0.5% in the BIO scenario. Increases in 24-h average ozone levels of 1–2 ppb occur north of Los Angeles in locations near the Angeles National Forest and around Hesperia. Both these regions have mountainous or rural terrain with a high density of plant life. Only areas located near or downwind of biogenic emission sources that are close enough to source of anthropogenic NO_X emissions are impacted in the BIO scenario. Highly urbanized areas such as Los Angeles and costal locations such as Long Beach are not affected by increased isoprene emissions due to their geographic location relative to the sources of these emissions. Millstein and Harley (2009) also reported that ozone concentrations were the most impacted by increased biogenic emissions in areas north and east of Los Angeles.

3.1.4. Impact of boundary conditions

In the BC scenario, increasing chemical boundary conditions of O₃, NO, and NO₂ at the western inflow causes afternoon domain wide average ozone concentrations to increase by about 5%. The impact of the BC scenario on peak afternoon ozone levels at the individual locations examined in Table 3 exhibits a high degree of spatial dependence. Newhall, Anaheim, and Long beach are the most impacted cities in the BC scenario. All three cities are located near and directly downwind of the western boundary (see Fig. 1). The influence of changes to western inflow boundary conditions diminishes as one moves inland from the coast and typically only reaches as far inland as Riverside. Millstein and Harley (2009) and Steiner et al. (2006) both found that the largest ozone increases occur for locations in close proximity to the western model boundary and that the extent of the impact decreases as air is transported eastward.

Fig. 2c shows not only the impact of changing boundary conditions on ozone concentrations but also the predominant summer wind patterns present in the SoCAB. Contours show the typical trajectory of air parcels as they are advected inland from the Pacific and the resulting impact on air quality for inland portions of the basin. As expected, the largest increases in 24-h average ozone concentrations in the BC scenario occur adjacent to the western boundary or directly inland. For example, inland areas west of Los Angeles experience 24-h average ozone increases of 5-12 ppb. The northeast portion of the basin, which is generally the most affected by climate related perturbations, experiences no change in ozone concentrations from changes in western inflow boundary conditions. Overall, the BC perturbation scenario results in significant increases to both afternoon and 24-h average ozone concentrations for areas west of Los Angeles and south of Anaheim, while the inland portion of the basin remains unaffected.

3.1.5. Combined effects

Some of the combined scenarios with simultaneous perturbations to more than one parameter have results that closely resemble linear combinations of individual perturbation scenarios. Other combined scenarios indicate compensating or compounding effects when more than one parameter is perturbed simultaneously in the same model run. In the latter case, the resulting impact on air quality is much different than what would be expected from the sum of the individual scenarios. This illustrates the highly coupled nature of different meteorological variables and their impact on ozone air quality. Various combinations of temperature, humidity, biogenic emission, and boundary condition perturbations are considered to elucidate any interactions amongst the parameters.

In the HTEMP + HUMID scenario, the change in afternoon, domain wide average, and 24-h average ozone concentrations is essentially the same as that seen in the HTEMP scenario (see Table 2). Ozone concentrations increase more in the HTEMP + BIO scenario than in the HTEMP scenario, and the change in afternoon, domain wide average, and 24-h average ozone concentrations is essentially equal to the sum of changes in the individual HTEMP and BIO scenarios for both emissions cases.

In the HTEMP + HUMID + BIO scenario, the impact on ozone behaves as the sum of changes from the HTEMP + HUMID scenario and the BIO scenario. The effect of increased biogenic emissions on ozone air quality does not appear to be influenced by simultaneous changes in humidity. This applies to both afternoon domain wide average values and afternoon ozone concentrations at specific locations in both emissions cases. Increases in peak afternoon ozone concentrations shown in Table 3 for the HTEMP + HUMID + BIO scenario are in agreement those projected by Millstein and Harley (2009). They showed ozone increases of 3–15 ppb as a result of simultaneous perturbations to temperature, humidity and biogenic

emissions. They also indicated that the largest increases occur further inland, particularly near Riverside.

The greatest impact on ozone air quality comes from the HTEMP + HUMID + BIO + BC scenario with simultaneous perturbations to all parameters. Ozone concentrations increase more in this scenario than in any other perturbation scenario. Even with reduced precursor emissions in the 2023 case, afternoon domain wide average ozone concentrations increase by about 10 ppb. Although specific locations exhibit varying sensitivity to the HTEMP + HUMID + BIO + BC scenario, all locations experience afternoon ozone increases of about 10% or more when using 2023 emissions and about 20% or more when using 2005 emissions. The most impacted areas are those susceptible to both climate related perturbations and changes in boundary conditions. Proximity to the western boundary and geographic location relative to biogenic and anthropogenic emission sources are largely responsible for determining the impact of the HTEMP + HUMID + BIO + BC scenario on local air quality. Data presented in Table 3 demonstrates this spatial dependence and shows the relative contribution of each perturbation to ozone increases at any given location.

24-h Changes in average ozone in the HTEMP + HUMID + BIO + BC scenario are shown in Fig. 2d. Few areas are susceptible to both climate related perturbations and perturbations to boundary conditions. When using 2023 emissions, 24-h average ozone concentrations increase by at least 10 ppb for much of the domain. Increases in 24-h average ozone concentrations and afternoon domain wide average ozone concentrations are similar in magnitude. This indicates that the penalty to ozone air quality occurs on large temporal and spatial scales. Future climate change is likely to cause significant increases in ozone concentrations across the domain not only during the afternoon hours, but throughout the day.

3.2. Particulate matter

The impact of the perturbations considered in Table 1 on ground-level PM concentrations differs greatly from the impact on ozone concentrations. Furthermore, the effect of each perturbation on PM varies depending upon the PM component considered. For example, the temperature dependence of sulfate and nitrate particulates are of opposite sign. Sulfate particulate concentrations increase with increasing temperature due to faster SO₂ oxidation while nitrate and organic semi-volatile particulates shift from the particle to the gas phase under higher temperature conditions (Jacob and Winner, 2009). Ammonium particles respond to temperature perturbations similar to nitrate. Their concentrations decrease with increasing temperature. Previous studies have also shown increased formation of ammonium nitrate under higher relative humidity conditions (Kleeman, 2008; Tai et al., 2010). In the SoCAB, changes in total PM concentrations for all perturbation scenarios are due primarily to the dominating presence of ammonium nitrate in the particles. Nitrate is the major PM component in the region. Therefore, the overall effect of different perturbation scenarios on total PM concentrations is dominated by changes in nitrate particulate concentrations. Also, the spatial distribution of total PM change for any perturbation scenario versus the base case closely resembles the change in nitrate PM, as shown in Fig. 3 for the HTEMP + HUMID + BIO + BC scenario. Ammonium particulates are another major contributor to total PM and the spatial distribution of changes in ammonium PM also closely follows changes in total PM for all perturbation scenarios (see Fig. 3c). This is expected due to the dominating presence of ammonium nitrate that disassociates to form ammonium (NH_4^+) and nitrate (NO_3^-) ions in the particle phase. Sulfates (SO_4^{2-}) also contribute considerably to peak PM concentrations in some areas but are not well distributed

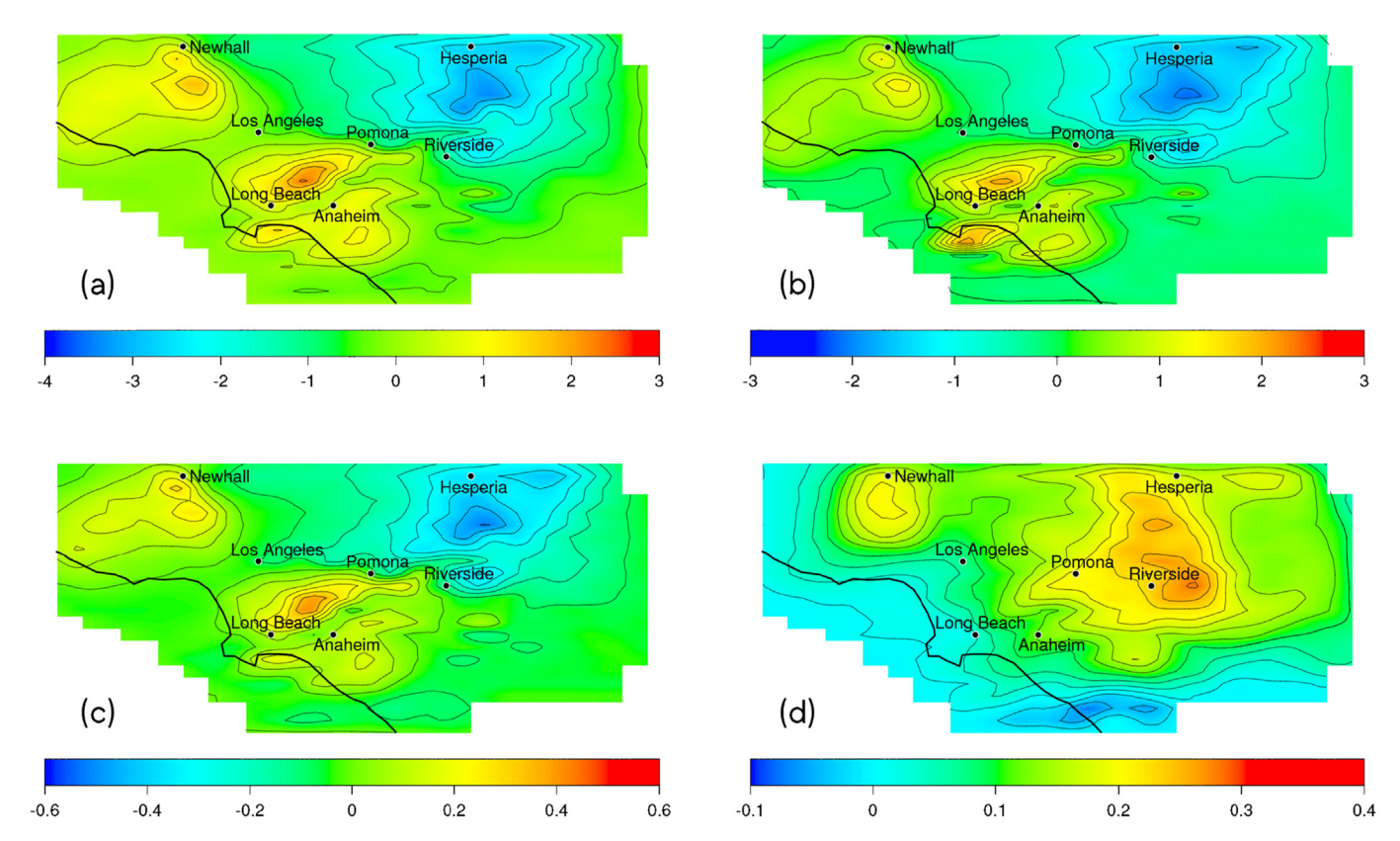


Fig. 3. Differences between future and base case 24-h average PM_{10} concentrations ($\mu g/m^3$) in the HTEMP + HUMID + BIO + BC scenario using 2023 emissions for (a) total PM_{10} , (b) nitrate (NO_3^-) PM_{10} , (c) ammonium (NH_4^+) PM_{10} , and (d) sulfate (SO_4^{2-}) PM_{10} . Positive values represent increases in concentration with respect to the base case.

throughout the domain. Precursor emissions of SO₂ are primarily due to ships and thus are located along the coast in shipping lanes and around the Port of Long Beach. As a result, high sulfate particulate concentrations occur only in isolated areas and the spatial distribution of changes in sulfate PM does not resemble changes in total PM as shown in Fig. 3d. Other inorganics such as chlorine, sodium, and crustal species contribute notably to total PM base case levels, but exhibit little to no change in concentrations from the perturbations considered in Table 1. Oxygenated polycyclic aromatic hydrocarbons (PAH) also contribute significantly to total PM concentrations in the base case. However, they too are insensitive to the perturbations considered in this study. Together, changes in nitrate and ammonium particulate concentrations account for approximately 75% of the change in total PM₁₀ concentrations in all perturbation scenarios for both emissions cases. Dawson et al. (2007b) reach a similar conclusion for many cities in their Eastern United States modeling domain. They found that changes in total PM_{2.5} closely resemble changes in nitrate PM_{2.5} in both magnitude and distribution. Although peak, afternoon, and 24-h average PM concentrations are lower when using 2023 emissions than when using 2005 emissions, the spatial distribution of changes in nitrate, sulfate, ammonium, and total PM is similar in all perturbation scenarios for both emissions cases.

In terms of particle size, PM_{10} and $PM_{2.5}$ exhibit similar dependence on meteorological variables. Modeled base-case $PM_{2.5}$ concentrations are about 60-70% of those of PM_{10} (see Tables 2 and S1), indicating a large presence of fine particulates which are known to pose a greater risk to public health (Ebi and McGregor, 2008). The portion of fine particles predicted in the model are in agreement with that measured by Kim et al. (2000) who determined that 52-59% of PM_{10} in the SoCAB is in the $PM_{2.5}$ fraction on

an annual average basis. Because fine particles comprise the majority of total PM₁₀, changes in PM₁₀ levels closely resemble changes in PM_{2.5} in both magnitude and distribution, as shown in Fig. 4a and b. Tables 4, S4, S2, and S3 present base-case PM₁₀ and PM_{2.5} levels at 16:00 h for key locations in the basin, as well as the change in afternoon PM concentrations that occurs in each perturbation scenario. The model predicts peak base case 24-h average PM_{2.5} concentrations of 115–130 μ g/m³ in the Riverside area, with coastal concentrations in the $20-40 \mu g/m^3$ range when using 2005 emissions (see Fig. 5a). Both the magnitude and distribution of base case 24-h average PM_{2.5} levels are in good agreement with those predicted by Aw and Kleeman (2003). They showed peak 24-h average PM_{2.5} concentrations of 125 μ g/m³, with the highest concentrations northeast of Riverside and lower concentrations occurring in coastal regions. Using 2023 emissions reduces base case PM₁₀ and PM_{2.5} levels, although the distribution remains the same (see Fig. 5b). Smaller particles exhibit the greatest sensitivity to all the perturbations considered, while particles with aerodynamic diameters between 2.5 μm and 10 μm are generally less affected. Thus, the spatial distribution of changes in PM₁₀ and PM_{2.5} concentrations is similar for all perturbation cases and the behavior of PM₁₀ is representative of the overall response of total PM air quality to the perturbations considered. Furthermore, while peak PM concentrations typically occur in the morning (3:00 h-7:00 h), the largest changes in PM concentrations for both particle sizes occur during the afternoon hours (13:00 h-17:00 h), similar to ozone. Therefore, changes in afternoon PM concentrations presented in the tables are for 16:00 h LT. Because changes in PM for most perturbation scenarios are not largely influenced by the emissions inventory utilized, results that follow are for the 2023 emissions case only, unless otherwise noted.

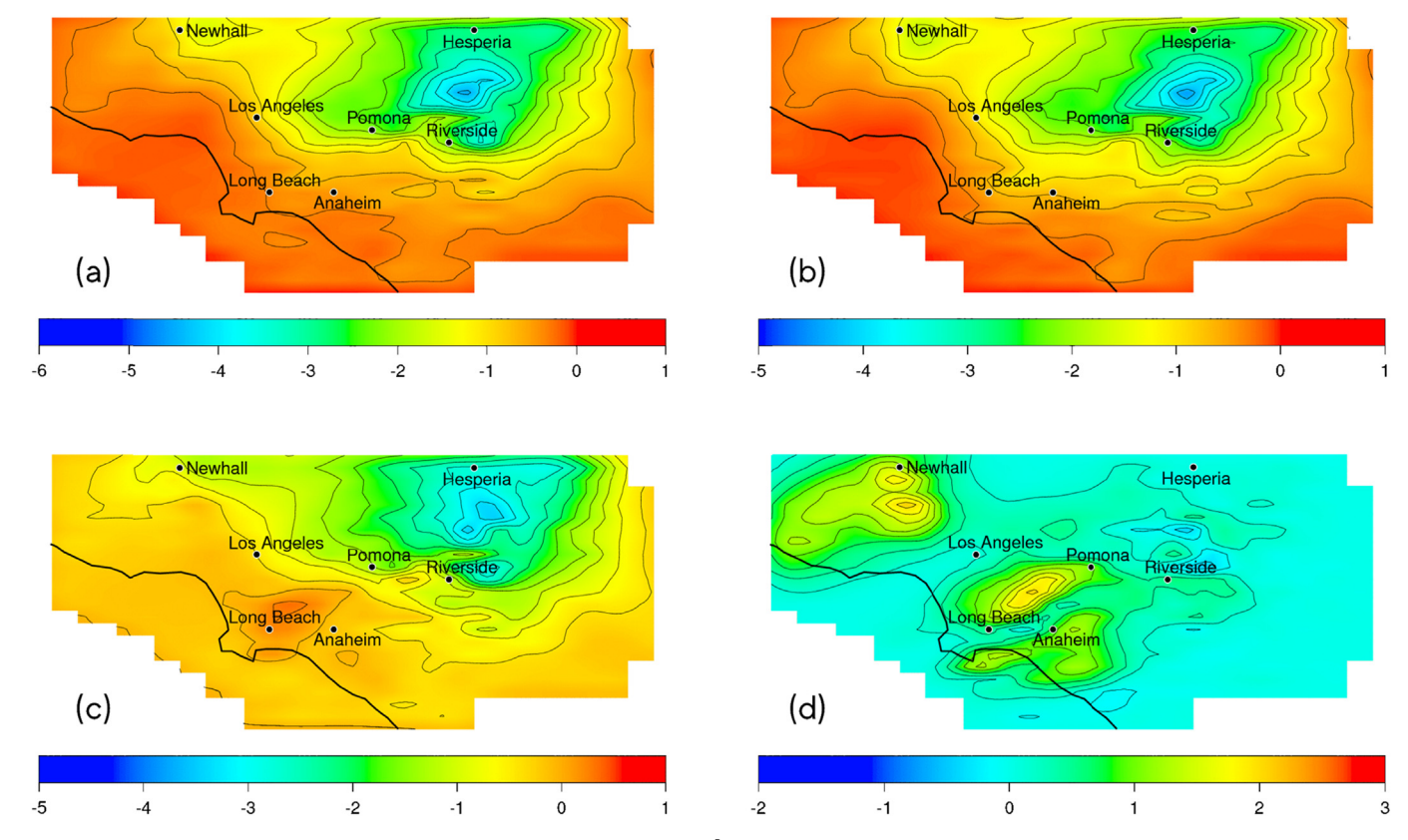


Fig. 4. Differences between future and base case 24-h average PM concentrations (μg/m³) using 2023 emissions for (a) total PM₁₀ in the HTEMP scenario, (b) total PM_{2.5} in the HTEMP scenario, (c) total PM₁₀ in the HTEMP + HUMID + BIO scenario, and (d) total PM₁₀ in the BC scenario. Positive values represent increases in concentration with respect to the base case

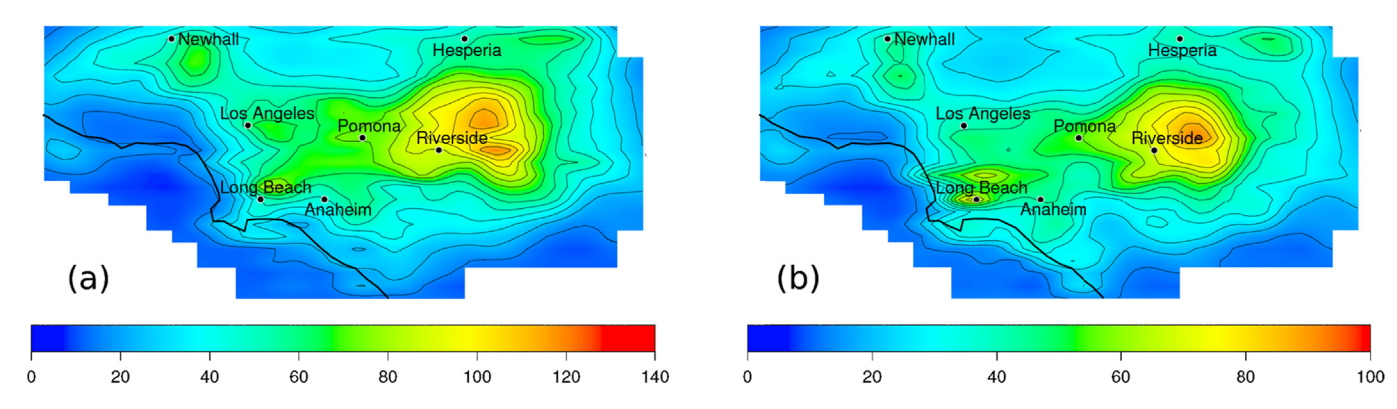


Fig. 5. Base case 24-h average PM_{2.5} concentrations (μ g/m³) (a) using 2005 emissions and (b) using 2023 emissions.

3.2.1. Impact of temperature

When only temperature is perturbed, the effect of increasing temperatures is to decrease PM concentrations throughout most the domain for both $PM_{2.5}$ and PM_{10} . The decrease in domain wide average afternoon PM concentrations for the LTEMP and HTEMP scenarios is similar for fine and coarse particles (see Table 2). Thus, the change in $PM_{2.5}$ concentrations is responsible for the majority of the decrease in total PM_{10} levels. Examining the change in afternoon PM concentrations at specific locations throughout the domain in Table 4 highlights the varying sensitivity of different microclimates and PM components to temperature perturbations. PM levels in coastal areas such as Long Beach and remote locations like Palm Springs, for example, exhibit little sensitivity to changes in temperature with decreases in afternoon PM_{10} levels of less than

1%. Conversely, areas such as Hesperia and Pomona show decreases in afternoon PM concentrations of 8.9% and 7.9%, respectively, for the HTEMP scenario. Both of these locations are downwind of strong NO_X emissions sources and experience significant decreases in nitrate particulates when temperatures are increased. While Newhall and Hesperia both display the same base-case afternoon PM_{10} concentration of 45 $\mu g/m^3$, Newhall shows only a 3.5% decrease in afternoon PM_{10} levels for the HTEMP scenario. PM composition in Newhall differs from that in Hesperia and Pomona due to its location in the basin, resulting in a different response to temperature increases. Newhall is not heavily influenced by anthropogenic NO_X emissions. Therefore, it does not experience the same large decreases in nitrate and total PM as Pomona and Hesperia. The sensitivity of PM to temperature changes is nonlinear. In

Table 4 PM_{10} concentration ($\mu g/m^3$) for select locations at 16:00 h LT using 2023 emissions: Base case levels shown in top row. Difference and percent difference in PM_{10} concentration between the specified perturbation scenario and the base case shown in bottom rows. Positive values represent increases in concentration with respect to the base case. The dash (–) indicates that the difference is less than the number of significant figures shown (i.e., less than 0.1 change from base case levels).

Base Case PM ₁₀	Los Angeles	Riverside	Anaheim	Pomona	Newhall	Long Beach
	31	62	32	92	45	36
LTEMP	-0.4, -1.3%	-0.9, -1.5%	-0.5, -1.5%	-1.5, -1.7%	-0.7, -1.7%	-0.1, -0.2%
HTEMP	-0.8, -2.5%	-2.5, -4.1%	-0.5, -1.6%	-7.3, -7.9%	-1.6, -3.5%	-0.3, -0.9%
HUMID	0.2, 0.5%	0.4, 0.6%	0.1, 0.2%	2.5, 2.7%	-0.1, -0.3%	0.2, 0.6%
BIO	-	-0.1, -0.1%	-0.3, -0.8%	0.1, 0.1%	-0.6, -1.3%	-0.1, -0.3%
HTEMP + HUMID	-0.5, -1.7%	-2.4, -3.8%	-0.5, -1.5%	-4.8, -5.2%	-1.5, -3.2%	-0.1, -0.3%
HTEMP + BIO	-0.9, -2.9%	-2.8, -4.6%	-0.6, -1.9%	-5.5, -5.9%	-1.8, -3.9%	-0.4, -1.1%
HTEMP + HUMID + BIO	-0.6, -2.1%	-2.5, -4.0%	-0.8, -2.4%	-4.5, -4.9%	-1.8, -4.1%	-0.1, -0.3%
BC	0.3, 0.9%	0.5, 0.8%	_	0.3, 0.3%	0.9, 2.0%	0.5, 1.3%
HTEMP + HUMID + BIO + BC	-0.3, -0.9%	-2.5, -4.1%	-	-4.8, -5.2%	-0.8, -1.7%	0.6, 1.7%

Pomona, for example, afternoon PM_{10} levels decrease by only 1.7% in the LTEMP scenario, but decrease by 8.9% in the HTEMP scenario.

In conclusion, areas that are downwind of strong NO_X emissions sources and contain sufficient gas phase ammonia for the formation of ammonium nitrate are the most impacted by temperature increases. This conclusion was also observed by Aw and Kleeman (2003), who reported that ammonium nitrate concentrations are most sensitive to temperature perturbations in areas that contain comparable molar concentrations of gas-phase ammonia and nitric acid. Conversely, ammonium nitrate particles exhibit little sensitivity to changes in temperature when the ratio of gas-phase ammonia to nitric acid is much greater or much less than unity (Aw and Kleeman, 2003). Dawson et al. (2007b) also found significant decreases in nitrate and ammonium particulates during the summer in response to temperature increases, due mostly to the volatilization of ammonium nitrate.

Fig. 4 shows changes in 24-h average PM_{10} and $PM_{2.5}$ concentrations for the HTEMP scenario. Areas north of Riverside are the most affected, with decreases in 24-h average PM_{10} and $PM_{2.5}$ concentrations of $2-5~\mu g/m^3$. Areas along the coast experience little to no reduction in PM levels. These results are similar to those predicted by Aw and Kleeman (2003). They showed reductions in inland 24-h average $PM_{2.5}$ concentrations of 2.5 $\mu g/m^3$ or more in response to temperature increases, with the greatest reductions occurring in the northeast portion of the basin.

3.2.2. Impact of humidity

In the HUMID scenario, domain wide average afternoon PM concentrations show slight increases compared to base case levels (see Table 2). Results are similar for the specific locations examined in Table 4 where most locations show less than 1% change from base case levels. There are increases in 24-h average PM₁₀ concentrations of $1-2 \mu g/m^3$ for the central area of the domain around Pomona with the greatest increases occurring further inland, directly north of Riverside. Because these increases are isolated to a small portion of the basin, the overall increase in PM concentrations for the entire domain is small. Increases in nitrate and ammonium account for nearly all of the change in total PM when humidity is increased. Sulfate particulates also exhibit a positive response to the HUMID scenario, although the increase in 24-h average concentrations is small ($<0.2 \mu g/m^3$) and isolated to areas downwind of strong SO₂ emission sources. Overall, atmospheric particulates show a weak but generally positive response to increases in both absolute and relative humidity. Our results are consistent with Dawson et al. (2007b) and Kleeman (2008) who found that PM concentrations increase with increasing concentration of water vapor. Moreover, they showed that increasing absolute humidity had the largest impact on ammonium nitrate particulate concentrations due to the ammonia-nitric acid system shifting toward the aerosol phase (Dawson et al., 2007b; Kleeman, 2008).

3.2.3. Impact of biogenic emissions

PM concentrations in the SoCAB exhibit little sensitivity to changes in biogenic emissions. The change in PM levels for the BIO scenario is essential zero when looking at afternoon domain wide average values. Newhall, which is near strong sources of isoprene coming from the Angeles National Forest, shows the greatest change: a 1.3% decrease in afternoon PM levels. This decrease can be attributed to reduced nitrate particulate concentrations. The reduction in nitrate concentrations results from NO_X scavenging by isoprene. This, combined with the already reduced NO_X emissions in the 2023 case, significantly decreases the potential to form nitric acid and nitrate particulates. A few isolated locations near isoprene emission sources north and east of Riverside experience changes in 24-h average PM concentrations of 0.5 $\mu g/m^3$, while most of the domain remains unaffected.

3.2.4. Impact of boundary conditions

Perturbing boundary conditions in the BC scenario has little effect on PM concentrations. Afternoon domain wide average PM_{10} and $PM_{2.5}$ concentrations increase by less than 1% in both emissions cases. Individual locations examined in Table 4 behave similarly. Small increases in afternoon PM concentrations occur for some locations due to the increased inflow of NO_X at the western boundary.

Increases in 24-h average PM concentrations shown in Fig. 4d range from 1 to 2 μ g/m³ in impacted areas. Orange and Los Angeles counties are the most affected, with the largest increases occurring around Anaheim and northwest of Los Angeles. As was the case with ozone, the impact of perturbing boundary conditions does not reach the far northern or eastern portions of the basin, so areas north or east of Riverside experience little to no change in PM for the BC scenario. Increases in ammonium nitrate PM that result from higher NO_X boundary conditions are responsible for essentially all of the increase in total PM levels in the BC scenario.

3.2.5. Combined effects

In general, temperature increases play the principal role in determining the impact on PM air quality in the combined perturbation scenarios. In the HTEMP + HUMID scenario, changes in afternoon domain wide average PM levels behave as a linear combination of the effects seen in the individual HTEMP and HUMID scenarios. The increase in PM levels that occurs the HUMID scenario offsets some of the decrease seen in the HTEMP scenario, causing PM levels to decrease less in the HTEMP + HUMID scenario than in the HTEMP scenario. The specific locations examined in Table 4 exhibit similar behavior. These results are consistent with

Kleeman (2008) who showed that the negative temperature effect on $PM_{2.5}$ concentrations is greater in magnitude than the positive humidity effect.

The spatial distribution of changes in 24-h average PM concentrations in the combined HTEMP + HUMID scenario closely resemble those seen in the HTEMP scenario (Fig. 4a,b), though PM levels decrease by about 1 µg/m³ less in the combined scenario. Overall, results are in agreement with Kleeman (2008) who predicted decreases in PM_{2.5} concentrations of 1–7 µg/m³ in most inland portions of the basin when temperatures were increased with no change in relative humidity. The differences between the combined HTEMP + HUMID scenario and the individual HTEMP scenario can be attributed to the increase in absolute humidity in the combined scenario, since relative humidity remains equal to that in the base case for combined scenario. Increasing absolute humidity results in higher concentrations of ammonium nitrate aerosol due to the equilibrium of the ammonia-nitric acid system being shifted toward the aerosol phase (Dawson et al., 2007b; Kleeman, 2008). This effect partially offsets some of the decrease in ammonium nitrate concentrations that results from increased volatilization at higher temperatures.

In the HTEMP + BIO scenario, the change in domain wide average afternoon PM concentrations is essentially the same as that seen in the HTEMP scenario. Similarly, when averaged over a 24-h period, both the magnitude and distribution of changes in PM concentrations for the HTEMP + BIO scenario are nearly identical to that seen in the HTEMP scenario in Fig. 4a,b.

Temperature is also the most significant perturbation that affects PM in the HTEMP + HUMID + BIO scenario. The change in afternoon domain wide average PM concentrations for the combined HTEMP + HUMID + BIO scenario is only 0.1 $\mu g/m^3$ different than the changes seen in the HTEMP + HUMID and HTEMP scenarios. The change in PM levels in this combined scenario at individual locations closely resembles the sum of changes from the three individual (HTEMP, HUMID and BIO) perturbation scenarios. Any apparent interactions among the three perturbation parameters are those discussed previously for the HTEMP + HUMID scenario.

When all perturbations are considered simultaneously in the HTEMP + HUMID + BIO + BC scenario, the effect of increasing temperatures still dominates the overall impact on afternoon PM concentrations, resulting in a 3% reduction in afternoon domain wide average PM levels. The change in PM concentrations for most of the specific locations examined in Table 4 behaves as a linear combination of the changes seen in the HTEMP + HUMID + BIO scenario and the BC scenario. The change in PM concentrations at most locations is due primarily to either changes in boundary conditions or increased temperature, humidity, and biogenic emissions, based on geographic location in the basin. For example, in Long Beach and Anaheim, afternoon PM concentrations increase in the HTEMP + HUMID + BIO + BC scenario due to the strong influence of boundary conditions and limited effect of temperature increases.

The change in 24-h average PM concentrations for the HTEMP + HUMID + BIO + BC scenario is a strong function of location in the basin, as shown in Fig. 3a. Areas near the coast, particularly those around Anaheim and Long Beach and south of Newhall, experience increases in 24-h average PM concentrations of $1-2.5~\mu g/m^3$ due to changes in boundary conditions. Because of their proximity to the ocean and relatively low base case temperatures, these coastal areas do not experience significant decreases in ammonium nitrate PM from temperature perturbations. They are, however, susceptible to increased NO_X concentrations at the western boundary, promoting the formation of nitric acid and nitrate PM. Increases in nitrate particulate concentrations account for

nearly all the increase in total PM_{10} in these areas, as shown in Fig. 3b. Areas located further inland and north of Riverside show 24-h average PM decreases of $2-4~\mu g/m^3$. In this portion of the basin, base case temperatures are already high and the effect of increasing temperatures further causes large reductions in nitrate and ammonium PM (see Fig. 3b,c). Comparing Fig. 4c to d illustrates how climate related perturbations and changes in boundary conditions generally impact different portions of the basin. Overall, 24-h average PM concentrations increase in coastal areas due to changes in boundary conditions and decrease in the northeastern portion of the SoCAB due primarily to the temperature increase.

3.3. Secondary organic aerosols

3.3.1. Impact of temperature

Both the LTEMP and the HTEMP perturbation scenarios cause significant reductions in SOA concentrations during the afternoon hours (14:00 h-17:00 h). SOA levels decrease less during the early morning (1:00 h-5:00 h) and late night hours (20:00 h-24:00 h), though the effect of increasing temperatures is consistently negative. Higher temperatures result in decreased gas to particle partitioning in equilibrium partitioning models due to the effects of temperature on Henry's law coefficients and vapor pressure (Griffin et al., 2005). VOCs tend to favor the gas phase as temperatures increase, decreasing SOA yield. These effects are strongest during daytime and afternoon hours when base case temperatures are already high. Overall, the effect of increasing temperatures by 3 °C is to decrease afternoon SOA concentrations by approximately 20% for much of the domain. Both the percentage change and spatial distribution of changes in SOA concentrations is similar for 2005 and 2023 emissions cases even though base case SOA levels are lower in some locations when emissions are reduced in the 2023 case (see Table 5 and S6). As an example, base-case afternoon SOA levels in Riverside are 11.0 μ g/m³ and 7.3 μ g/m³ when using 2005 emissions and 2023 emissions, respectively. However, the percentage change in afternoon SOA concentrations for the HTEMP scenario is similar for both emissions cases: a 20.8% and 22.6% decrease for 2005 and 2023 emissions cases, respectively.

The spatial distribution of changes in 24-h average SOA concentrations is similar to changes in afternoon SOA levels at 16:00 h, as shown in Fig. 6a,b. One notable difference is the presence of large decreases in afternoon SOA concentrations north of Los Angeles near Newhall that are not present when concentrations are averaged over a 24-h period. SOA concentrations in this area are most sensitive to temperature increases during daytime and afternoon compared with nighttime. Time series data for SOA concentrations in Newhall confirms this trend, showing that hourly SOA concentrations decrease by only 1-3% from 1:00 h-8:00 h and 3-6% from 20:00 h-24:00 h. compared with decreases of 15-21% from 12:00 h-18:00 h. As was the case with PM, coastal regions experience little to no change in afternoon and 24-h average SOA levels, while areas further inland show significant reductions in both afternoon and 24-h average SOA concentrations as temperature increases. This is expected due to the transport of the precursors required to form SOA to downwind areas of the basin and the relatively low base-case temperatures near the coast.

3.3.2. Impact of humidity

The HUMID perturbation scenario causes small increases in both afternoon and 24-h average SOA concentrations. For the domain as a whole, SOA concentrations increase by 3.2% and 2.0% when using 2005 and 2023 emissions, respectively. When using 2023 emissions, afternoon increases are similar in magnitude though more localized than the 2005 emissions case, with the largest increases occurring around Pomona (see Fig. 6c). Areas with high base-case

Table 5 SOA concentration ($\mu g/m^3$) for select locations at 16:00 h LT using 2023 emissions. Base case levels shown in top row. Difference and percent difference in SOA concentration between the specified perturbation scenario and the base case shown in bottom rows. Positive values represent increases in concentration with respect to the base case. The dash (–) indicates that the difference is less than the number of significant figures shown (i.e., less than 0.1 change from base case levels).

Base Case SOA	Los Angeles	Riverside	Anaheim	Pomona	Newhall	Long Beach
	3.6	7.3	2.4	13.1	4.3	1.5
LTEMP	-0.2, -4.8%	-0.6, -7.6%	-0.1, -5.0%	-0.5, -3.6%	-0.3, -7.5%	_
HTEMP	-0.5, -13.4%	-1.6, -22.6%	-0.3, -14.2%	-2.3, -17.7%	-0.8, -18.9%	-0.1, -6.1%
HUMID	0.2, 4.9%	_	0.1, 2.5%	0.7, 5.6%	_	0.1, 8.3%
BIO	-	-	-0.1, -4.4%	0.1, 1.0%	-0.1, -1.6%	
HTEMP + HUMID	-0.3, -8.3%	-1.6, -21.9%	-0.3, -13.8%	-2.0, -14.9%	-0.8, -19.3%	
HTEMP + BIO	-0.5, -13.5%	-1.7, -23.0%	-0.4, -15.2%	-2.3, -17.6%	-0.8, -18.9%	-0.1, -6.9%
HTEMP + HUMID + BIO	-0.3, -8.9%	-1.6, -21.9%	-0.3, -10.4%	-2.0, -14.9%	-0.8, -18.8%	
BC	0.1, 4.1%	-	-	0.2, 1.5%	-	0.1, 6.5%
HTEMP + HUMID + BIO + BC	-0.2, $-6.2%$	-1.6, -22.2%	-0.2, -7.5%	-2.0, -15.0%	-0.6, -14.5%	0.1, 3.7%

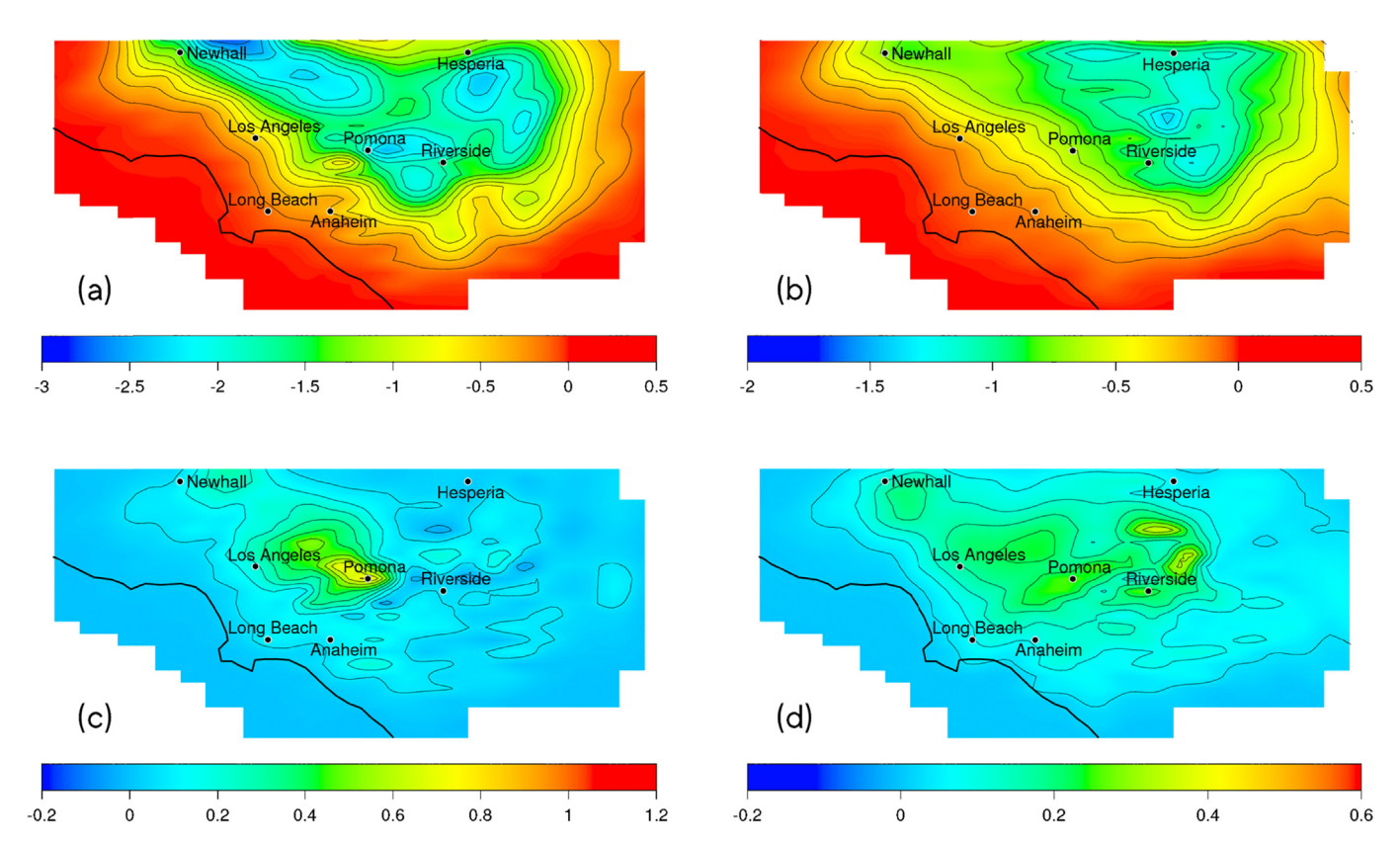


Fig. 6. Differences between future and base case SOA concentrations (μg/m³) when using 2023 emissions for (a) afternoon SOA at 16:00 h in the HTEMP scenario, (b) 24-h average SOA in the HTEMP scenario. Positive values represent increases in concentration with respect to the base case.

pollutant concentrations show the greatest sensitivity to humidity perturbations, while coastal areas are generally less impacted. Chang et al. (2010) also found that increases in relative humidity promote SOA formation, particularly in downwind areas of the basin where pollutants accumulate.

3.3.3. Impact of biogenic emissions

Increasing emissions of isoprene in the BIO scenario has essentially no effect on afternoon or 24-h average SOA levels in both emissions cases. Similarly, in the HTEMP + BIO scenario, the change in SOA concentrations is nearly identical to that seen in the HTEMP scenario.

3.3.4. Impact of boundary conditions

Perturbing boundary conditions in the BC scenario has little

effect on SOA concentrations for most of the domain. Afternoon domain wide average SOA concentrations change by 1% or less. The maximum change in afternoon SOA levels that occurs at the individual locations examined in Table 5 is 0.2 μ g/m³. Long Beach experiences the largest *relative* increase in SOA concentrations when using 2023 emissions since. Long Beach is directly downwind of the western boundary and has low base-case SOA levels. Here, afternoon SOA concentrations increase by 6.5% in the BC scenario when using 2023 emissions. The spatial distribution of changes in 24-h average SOA concentrations for the BC scenario, shown in Fig. 7b, is similar to that seen for PM in Fig. 4d. In both emissions cases, areas near Pomona, Anaheim, and Newhall experience increases in 24-h average SOA of 0.2–0.4 μ g/m³, while the remainder of the domain remains generally unaffected.

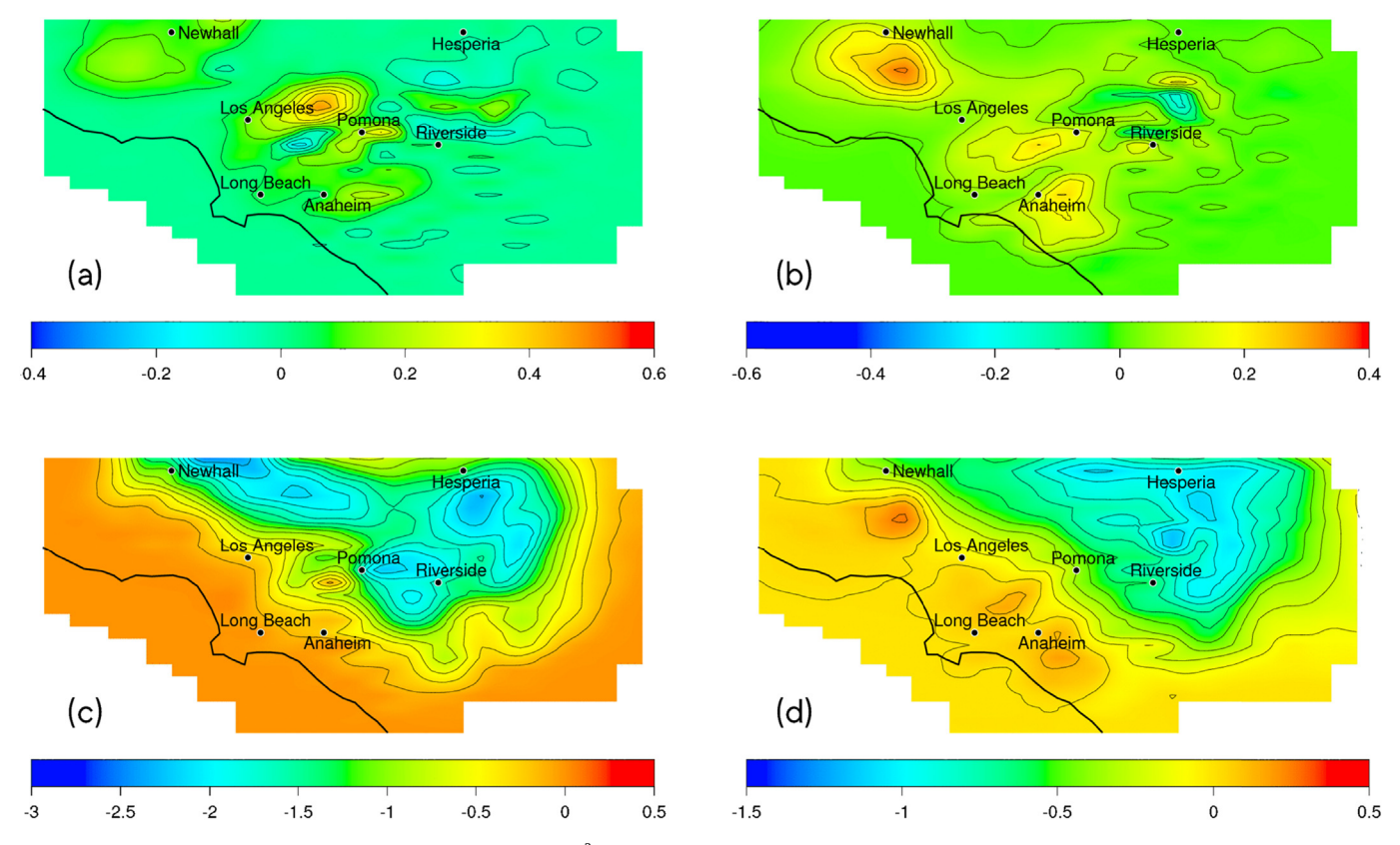


Fig. 7. Differences between future and base case SOA concentrations (μ g/m³) when using 2023 emissions for (a) afternoon SOA at 16:00 h in the BC scenario, (b) 24-h average SOA in the BC scenario, (c) afternoon SOA at 16:00 h in the HTEMP + HUMID + BIO + BC scenario, and (d) 24-h average SOA in the HTEMP + HUMID + BIO + BC scenario. Positive values represent increases in concentration with respect to the base case.

3.3.5. Combined effects

In the HTEMP + HUMID scenario, SOA concentrations decrease significantly throughout much of the domain. Here, the effect of increasing temperatures dominates. Qualitatively, the behavior is similar to that seen in Fig. 6a,b for the HTEMP scenario although there is evidence of compensating effects when temperature and absolute humidity area increased simultaneously. Table 2 shows that afternoon domain wide average SOA concentrations decrease less in the HTEMP + HUMID scenario than in the HTEMP scenario. Relative humidity remains the same as in the base case in the HTEMP + HUMID scenario. Therefore, it is primarily the change in absolute humidity that causes domain wide average SOA concentrations to increase in the HUMID scenario, and to decrease less in the HTEMP + HUMID scenario than in the HTEMP scenario. However, results for individual locations shown in Table 5 suggest that relatively humidity may also play a role in the response of SOA to the HTEMP + HUMID scenario in certain areas. Afternoon SOA concentrations in Pomona decrease by 2.3 µg/m³ in the HTEMP scenario and increase by 0.7 μ g/m³ in the HUMID scenario. In the HTEMP + HUMID scenario, afternoon SOA concentrations still decrease by 2.0 μ g/m³. Thus, part of the 0.7 μ g/m³ increase in SOA seen in the HUMID scenario is due to increased relative humidity and part is due to increase absolute humidity. Since relative humidity remains unchanged from the base case in the HTEMP + HUMID scenario, the 0.3 μ g/m³ difference in SOA change in Pomona for the HTEMP + HUMID scenario compared with the HTEMP scenario is attributed to increased absolute humidity. The spatial distribution of changes in 24-h average SOA concentrations for the HTEMP + HUMID scenario are nearly identical to those seen in Fig. 6b for the HTEMP scenario. The effect of perturbing temperature and humidity simultaneously is to reduce the magnitude of the impact of the temperature increase on SOA.

When emissions of isoprene are perturbed in addition to temperature and humidity in the HTEMP + HUMID + BIO scenario, results are nearly identical to the HTEMP + HUMID scenario. This is consistent with results for the BIO and HTEMP + BIO scenarios where SOA air quality exhibits little sensitivity to changes in biogenic emissions, even at higher temperatures.

In the HTEMP + HUMID + BIO + BC scenario, temperature dominates the change in domain wide average SOA levels. As a result, the change in afternoon domain wide average SOA concentrations in the $\overline{\text{HTEMP}} + \text{HUMID} + \text{BIO} + \text{BC}$ scenario is only a few percent different than that in all other scenarios involving the HTEMP perturbation (see Tables 5 and S5). Of the specific locations examined in Table 5, temperature increases in HTEMP + HUMID + BIO + BC scenario cause SOA levels to decrease in all areas except Long Beach. Here, the increase in SOA from perturbations to humidity and boundary conditions is greater than the decrease from rising temperatures, resulting in a 3.7% increase in SOA concentrations. In other areas such as Riverside and Hesperia, the decrease in SOA for the HTEMP + HUMID + BIO + BC scenario is similar to that seen in the HTEMP scenario. These inland areas exhibit little sensitivity to perturbations of humidity, biogenic emissions, and boundary conditions, even when the perturbations are considered simultaneously. SOA concentrations in Los Angeles and Anaheim are sensitive to many of the perturbations considered so that all perturbations contribute to the total change in afternoon SOA. However, the effect of increasing temperatures still dominates, causing SOA levels to decrease by over 6% in these two cities. Overall, temperature increases in the HTEMP + HUMID + BIO + BC scenario cause large reductions in afternoon SOA concentrations for all inland areas of the SoCAB (see Fig. 7c). This decrease is partially offset in some locations by simultaneously perturbing humidity and boundary conditions, though the response of SOA to the HTEMP + HUMID + BIO + BC scenario is still negative in nearly all areas in both emissions cases.

Changes in 24-h average SOA concentrations for the HTEMP + HUMID + BIO + BC scenario are shown in Fig. 7d. The response is qualitatively similar to that seen for PM₁₀ in the same perturbation scenario, Fig. 3a. Areas located further inland than Pomona experience decreases in 24-h average SOA concentrations of 0.5–1.5 μ g/m³ while isolated locations closer to the coast show increases of about 0.25 μ g/m³ when all perturbations are considered simultaneously in the HTEMP + HUMID + BIO + BC scenario.

4. Summary and conclusions

The overall impact of each perturbation scenario on ozone, PM, and SOA concentrations in the SoCAB is summarized in Fig. 8. Data presented in the figure is obtained by calculating mean and standard deviation of the change in domain wide average concentrations at each hour of day for an entire day of simulation. The change in domain wide average concentrations for each perturbation scenario versus the base case, averaged over this 24-h period, produces the colored bars on the figure. However, changes in the domain wide average concentration can vary significantly based on time of day, particularly for PM and SOA. The error bars extend one standard deviation above or below the mean, representing the amount of spread in the data due to the temporal dependence. Large error bars indicate that the impact of the perturbation scenario on air quality is a strong function of time of day. For example, when using 2005 emissions in the HTEMP + HUMID + BIO + BC scenario, PM₁₀ concentrations increase during the early morning hours, but decrease during the afternoon as temperatures in the basin rise. The mean change over 24-h is therefore small, though the standard deviation is large. Conversely, the increase in SOA concentrations in the HUMID scenario is consistent throughout the day, as indicated by the narrow error bars. Though Fig. 8 does not capture the spatial dependence of the perturbations, it provides a condensed view of the overall impact of each perturbation scenario on ozone, PM, and SOA concentrations in the SoCAB. Figure S2 in the supplementary material shows relative changes in concentration (%) rather than absolute changes in concentration shown in Fig. 8. Figure S2 reveals that although the magnitude of the change in domain wide average SOA concentrations shown in Fig. 8 is small, the relative changes are significant.

Fig. 9 shows the relative contribution of each individual perturbation to the total change in 24-h average ozone, PM₁₀, and SOA concentrations for select locations in the basin. The relative contribution of each individual perturbation is calculated following the methodology of He et al. (2016). That is, the relative contribution from each perturbation X_i % is defined as X_i % = $\frac{X_i}{\sum_i y_i} \times 100$ % where X_i represents the change in concentration in the individual HTEMP, HUMID, BIO, and BC scenarios. Fig. 9 illustrates the spatial dependence of the perturbations and shows the varying sensitivity of different microclimates to the perturbations considered in this study. For example, perturbing boundary conditions in the BC scenario contributes relatively more to changes in ozone concentration for areas near the coast compared with areas further inland. In Long Beach and Anaheim, changes in boundary conditions is responsible for almost 70% of the total change in ozone concentrations. Conversely, the relative contribution of the HTEMP scenario to the total change in ozone concentrations is lower for coastal areas than areas further inland. In Riverside, increasing temperatures contributes about 70% to the total change in ozone concentrations, while the BC scenario contributes less than 15%. Fig. 9 also indicates that the relative contribution of the HTEMP perturbation to the total change in SOA concentrations is greater than the contribution to the total change in PM₁₀ concentrations. Thus, while Fig. 8 summarizes the overall impact of each perturbation scenario on regional air quality for the basin as a whole, Fig. 9 provides insight on how each perturbation contributes to changes in local air quality.

The impact of increasing temperatures on air quality is greatest in the northeast portion of the domain where base case temperatures are already relatively high. Therefore, the largest changes in ozone, PM, and SOA concentrations that result from temperature perturbations occur in the same general area of the basin that is already burdened with poor air quality. However, the response of ozone to temperature increases is much different than the response of PM and SOA. Ozone concentrations increase with increasing temperatures due to faster reaction rates and decomposition of PAN while PM and SOA concentrations decrease, primarily due to increased hydrocarbon volatilization at higher temperatures. Higher temperatures also result in decreased gas to particle partitioning in equilibrium partitioning models due to the effects of temperature on Henry's law coefficients and vapor pressure (Griffin et al., 2005). PM and SOA levels generally increase slightly with increasing absolute humidity. Increasing humidity results in higher concentrations of ammonium nitrate aerosol due to the equilibrium of the ammonia-nitric acid system being shifted toward the aerosol phase (Dawson et al., 2007b; Kleeman, 2008). However, the response of ozone is weak and of variable sign. Under the more polluted conditions when using 2005 emissions, ozone concentrations generally increase by a few percent when humidity is perturbed. Conversely, when using 2023 emissions, precursor emissions and base-case pollutant concentrations are lower, leading to ozone increases in some areas and decreases in others. The largest changes in ozone, PM, and SOA concentrations that result from humidity perturbations occur directly north and west of Riverside, while areas near the edges of the domain remain generally unaffected. When using 2023 emissions, perturbing biogenic emissions has little impact on air quality. However, higher NO_X emissions present when using 2005 emissions cause isolated increases in ozone concentrations for locations near isoprene emissions sources, particularly in areas that are NO_X saturated. In the boundary condition perturbation scenario, ozone concentrations increase in offshore and coastal areas directly adjacent to the western boundary. In contrast, PM and SOA concentrations increase in areas further inland, particularly around Anaheim and northwest of Los Angeles. These increases for PM and SOA are due mostly to increased production of nitric acid and nitrate aerosol.

In all combined perturbation scenarios, temperature increases dominate the overall impact on ozone, PM and SOA. As a result, the largest changes in ozone, PM, and SOA concentrations for all combined scenarios occur in the northeastern portion of the basin where the effect of increasing temperatures is strongest. Perturbing absolute humidity, biogenic emissions, and boundary conditions offsets some of the decrease in PM and SOA concentrations that result from increasing temperatures. However, all of the perturbations tend to increase ozone concentrations. Thus, the largest changes in ozone concentrations occur in the combined scenario with simultaneous perturbations to all parameters. In contrast, the largest decreases in PM and SOA concentrations occur in the temperature only perturbation scenario.

Sensitivity to climate change parameters varies greatly based on geographic location, local emissions, chemical species of interest, time of day, as well as a host of other variables. The highly intertwined nature of variables such as temperature, humidity, and biogenic emissions results in competing and compounding effects

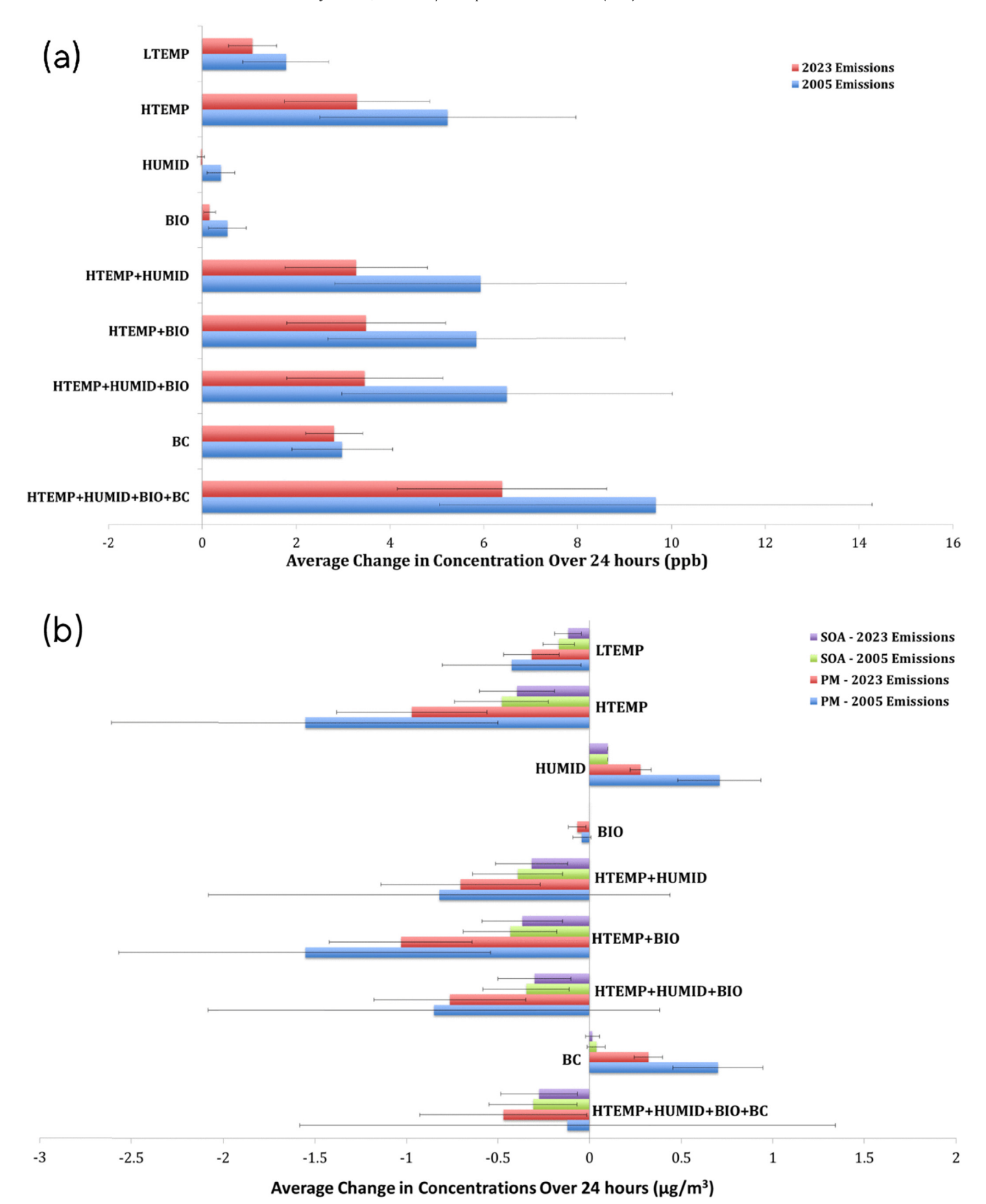


Fig. 8. Changes in domain wide average concentrations of (a) ozone and (b) PM₁₀ and SOA for each perturbation scenario in both emissions cases. Colored bars represent the average change in concentration over 24-h for the entire domain. Error bars indicate one standard deviation above or below the mean. Positive values represent increases in concentration with respect to the base case. (For interpretation of the references to colour in this figure legend, the reader is referred to the web version of this article.)

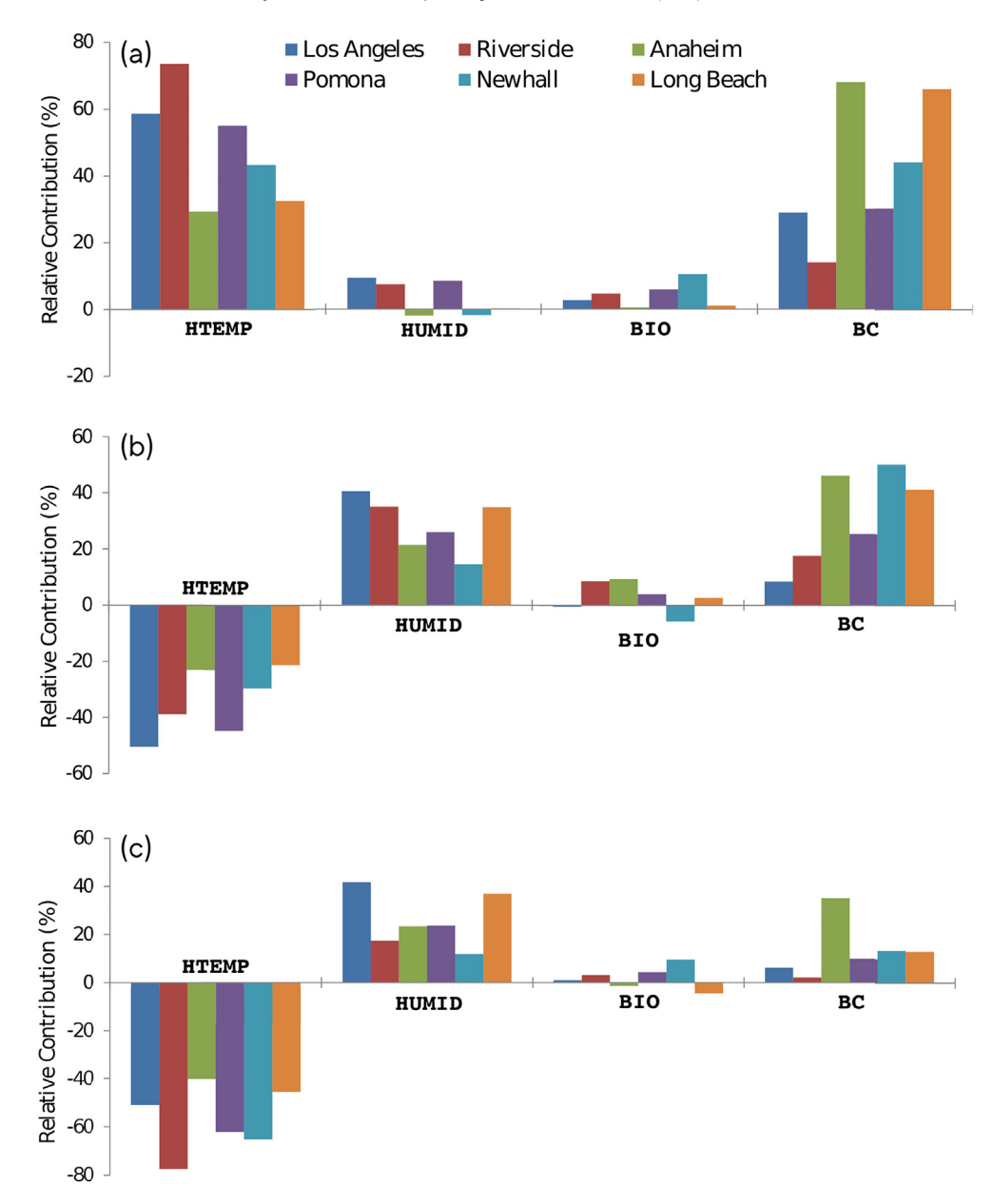


Fig. 9. Relative contribution of the individual perturbations considered in the HTEMP, HUMID, BIO, and BC scenarios to the total change in 24-h average concentrations of (a) ozone, (b) PM₁₀, and (c) SOA for select locations using 2023 emissions.

that can only be discovered with the detailed model approach employed. The use of a high-resolution regional air quality models with highly developed aerosol modules is necessary to study these effects on local air quality in California.

Previous studies have shown that temperature is the most important meteorological variable for determining the overall impact of future climate change on ozone concentrations (Aw and Kleeman, 2003; Steiner et al., 2006; Millstein and Harley, 2009; Jacob and Winner, 2009). Of all the perturbation scenarios considered in Table 1, those involving temperature have the greatest effects on ozone, PM, and SOA concentrations. This study shows that temperature increases play the dominant role in determining the overall impact of climate change on not only ozone, but also PM and SOA in both the individual and combined perturbation scenarios.

Air quality management strategies must consider these chemistry-climate interactions and their impact on pollutant concentrations. The potential air quality benefits of emission control policies and associated reductions in precursor emissions such as NO_X and VOCs may be offset by increasing temperatures or other climate change induced meteorological changes.

Acknowledgements

The authors would like to thank Professor Barbara J. Finlayson-Pitts and Professor Jacob Brouwer for providing their gracious feedback and insight during the revision process. This work was supported by the United States Environmental Protection Agency (EPA) [grant number 83588101].

Appendix A. Supplementary data

Supplementary data related to this article can be found at http://dx.doi.org/10.1016/j.atmosenv.2016.12.049.

References

- Aw, J., Kleeman, M.J., 2003. Evaluating the first-order effect of intraannual temperature variability on urban air pollution. J. Geophys. Res. Atmos. (1984—2012) 108 (D12).
- Brasseur, G.P., Schultz, M., Granier, C., Saunois, M., Diehl, T., Botzet, M., et al., 2006. Impact of climate change on the future chemical composition of the global troposphere. J. Clim. 19 (16), 3932—3951.
- Carreras-Sospedra, M., Griffin, R.J., Dabdub, D., 2005. Calculations of incremental secondary organic aerosol reactivity. Environ. Sci. Technol. 39 (6), 1724–1730.
- Carreras-Sospedra, M., Dabdub, D., Rodriguez, M., Brouwer, J., 2006. Air quality modeling in the south coast air basin of California: what do the numbers really mean? J. Air & Waste Manag. Assoc. 56 (8), 1184–1195.
- Carreras-Sospedra, M., Vutukuru, S., Brouwer, J., Dabdub, D., 2010. Central power generation versus distributed generation—an air quality assessment in the South Coast Air Basin of California. Atmos. Environ. 44 (26), 3215—3223.
- Chang, W.L., Griffin, R.J., Dabdub, D., 2010. Partitioning phase preference for secondary organic aerosol in an urban atmosphere. Proc. Natl. Acad. Sci. 107 (15), 6705–6710.
- Chock, D.P., Chang, T.Y., Winkler, S.L., Nance, B.I., 1999. The impact of an 8h ozone air quality standard on ROG and NO x controls in Southern California. Atmos. Environ. 33 (16), 2471–2485.
- Cohan, A., Eiguren-Fernandez, A., Miguel, A.H., Dabdub, D., 2013. Secondary organic aerosol formation from naphthalene roadway emissions in the South Coast Air Basin of California. Int. J. Environ. Pollut. 52 (3), 206–224.
- Cooper, O.R., Parrish, D.D., Stohl, A., Trainer, M., Nédélec, P., Thouret, V., et al., 2010. Increasing springtime ozone mixing ratios in the free troposphere over western North America. Nature 463 (7279), 344–348.
- Coquard, J., Duffy, P.B., Taylor, K.E., İorio, J.P., 2004. Present and future surface climate in the western USA as simulated by 15 global climate models. Clim. Dyn. 23 (5), 455–472.
- Dawson, J.P., Adams, P.J., Pandis, S.N., 2007a. Sensitivity of ozone to summertime climate in the eastern USA: a modeling case study. Atmos. Environ. 41 (7), 1494–1511.
- Dawson, J.P., Adams, P.J., Pandis, S.N., 2007b. Sensitivity of PM 2.5 to climate in the Eastern US: a modeling case study. Atmos. Chem. Phys. 7 (16), 4295–4309.
- Dawson, M.L., Xu, J., Griffin, R.J., Dabdub, D., 2016. Development of aroCACM/ MPMPO 1.0: a model to simulate secondary organic aerosol from aromatic precursors in regional models. Geosci. Model Dev. 9, 2143–2215.
- Ebi, K.L., McGregor, G., 2008. Climate change, tropospheric ozone and particulate matter, and health impacts. Environ. Health Perspect. 116 (11), 1449–1455.
- Ensberg, J.J., Carreras-Sospedra, M., Dabdub, D., 2010. Impacts of electronically photo-excited NO 2 on air pollution in the South Coast Air Basin of California. Atmos. Chem. Phys. 10 (3), 1171–1181.
- Gao, Y., Fu, J.S., Drake, J.B., Lamarque, J.F., Liu, Y., 2013. The impact of emission and climate change on ozone in the United States under representative concentration pathways (RCPs). Atmos. Chem. Phys. 13 (18), 9607–9621.
- Griffin, R.J., Dabdub, D., Seinfeld, J.H., 2002a. Secondary organic aerosol 1. Atmospheric chemical mechanism for production of molecular constituents. J. Geophys. Res. Atmos. (1984–2012) 107 (D17). AAC-3.
- Griffin, R.J., Dabdub, D., Kleeman, M.J., Fraser, M.P., Cass, G.R., Seinfeld, J.H., 2002b. Secondary organic aerosol 3. Urban/regional scale model of size-and composition-resolved aerosols. J. Geophys. Res. Atmos. 107 (D17).
- Griffin, R.J., Nguyen, K., Dabdub, D., Seinfeld, J.H., 2003. A coupled hydrophobic-hydrophilic model for predicting secondary organic aerosol formation. J. Atmos. Chem. 44 (2), 171–190.
- Griffin, R.J., Dabdub, D., Seinfeld, J.H., 2005. Development and initial evaluation of a dynamic species-resolved model for gas phase chemistry and size-resolved gas/ particle partitioning associated with secondary organic aerosol formation. J. Geophys. Res. Atmos. (1984–2012) 110 (D5).
- Grosjean, D., 2003. Ambient PAN and PPN in southern California from 1960 to the SCOS97-NARSTO. Atmos. Environ. 37, 221–238.
- Hayhoe, K., Cayan, D., Field, C.B., Frumhoff, P.C., Maurer, E.P., Miller, N.L., Moser, S.C., Schneider, S.H., Cahill, K.N., Cleland, E.E., Dale, L., 2004. Emissions pathways, climate change, and impacts on California. Proc. Natl. Acad. Sci. U. S. A. 101 (34), 12422–12427.
- He, H., Liang, X.Z., Lei, H., Wuebbles, D.J., 2016. Future US ozone projections dependence on regional emissions, climate change, long-range transport and differences in modeling design. Atmos. Environ. 128, 124–133.
- Heald, C.L., Henze, D.K., Horowitz, L.W., Feddema, J., Lamarque, J.F., Guenther, A., et al., 2008. Predicted change in global secondary organic aerosol concentrations in response to future climate, emissions, and land use change. J. Geophys. Res. Atmos. 113 (D5).
- Jacob, D.J., Winner, D.A., 2009. Effect of climate change on air quality. Atmos.

- Environ. 43 (1), 51-63.
- Jimenez, P., Baldasano, J.M., Dabdub, D., 2003. Comparison of photochemical mechanisms for air quality modeling. Atmos. Environ. 37 (30), 4179–4194.
- Kelly, J., Makar, P.A., Plummer, D.A., 2012. Projections of mid-century summer airquality for North America: effects of changes in climate and precursor emissions. Atmos. Chem. Phys. 12 (12), 5367–5390.
- Kleeman, M.J., 2008. A preliminary assessment of the sensitivity of air quality in California to global change. Clim. Change 87 (1), 273–292.
- Kim, B.M., Teffera, S., Zeldin, M.D., 2000. Characterization of PM25 and PM10 in the South Coast Air Basin of Southern California: Part 1—Spatial variations. J. Air & Waste Manag. Assoc. 50 (12), 2034–2044.
- Liao, H., Chen, W.T., Seinfeld, J.H., 2006. Role of climate change in global predictions of future tropospheric ozone and aerosols. J. Geophys. Res. Atmos. (1984–2012) 111 (D12).
- Lin, M., Fiore, A.M., Horowitz, L.W., Cooper, O.R., Naik, V., Holloway, J., et al., 2012. Transport of Asian ozone pollution into surface air over the western United States in spring. J. Geophys. Res. Atmos. 117 (D21).
- Lin, G., Penner, J.E., Zhou, C., 2016. How will SOA change in the future? Geophys. Res. Lett. 43, 1718–1726.
- Mahmud, A., Tyree, M., Cayan, D., Motallebi, N., Kleeman, M.J., 2008. Statistical downscaling of climate change impacts on ozone concentrations in California. J. Geophys. Res. Atmos. (1984–2012) 113 (D21).
- Mahmud, A., Hixson, M., Hu, J., Zhao, Z., Chen, S.H., Kleeman, M.J., 2010. Climate impact on airborne particulate matter concentrations in California using seven year analysis periods. Atmos. Chem. Phys. 10 (22), 11097—11114.
 Mahmud, A., Hixson, M., Kleeman, M.J., 2012. Quantifying population exposure to
- Mahmud, A., Hixson, M., Kleeman, M.J., 2012. Quantifying population exposure to airborne particulate matter during extreme events in California due to climate change. Atmos. Chem. Phys. 12 (16), 7453–7463.
- Marr, L.C., Harley, R.A., 2002. Modeling the effect of weekday-weekend differences in motor vehicle emissions on photochemical air pollution in central California. Environ. Sci. Technol. 36 (19), 4099–4106.
- Millstein, D.E., Harley, R.A., 2009. Impact of climate change on photochemical air pollution in Southern California. Atmos. Chem. Phys. 9 (11), 3745–3754.
- Nguyen, K., Dabdub, D., 2002. NO x and VOC control and its effects on the formation of aerosols. Aerosol Sci. Technol. 36 (5), 560–572.
- Ostro, B.D., Tran, H., Levy, J.I., 2006. The health benefits of reduced tropospheric ozone in California. J. Air & Waste Manag. Assoc. 56 (7), 1007–1021.
- Perera, E.M., Sanford, T., 2011. Rising Temperatures, Worsening Ozone Pollution. Pollack, I.B., Ryerson, T.B., Trainer, M., Neuman, J.A., Roberts, J.M., Parrish, D.D., 2013. Trends in ozone, its precursors, and related secondary oxidation products in Los Angeles, California: a synthesis of measurements from 1960 to 2010. J. Geophys. Res. Atmos. 118 (11), 5893–5911.
- Racherla, P.N., Adams, P.J., 2006. Sensitivity of global tropospheric ozone and fine particulate matter concentrations to climate change. J. Geophys. Res. Atmos. (1984–2012) 111 (D24).
- SCAQMD, Air Quality Management Plan (AQMP), 2007. Air quality management District (AQMD). Available at: http://www.aqmd.gov/home/library/clean-air-plans/air-quality-mgt-plan/2007-air-quality-management-plan (Accessed 15 May 2015).
- Snyder, M.A., Bell, J.L., Sloan, L.C., Duffy, P.B., Govindasamy, B., 2002. Climate responses to a doubling of atmospheric carbon dioxide for a climatically vulnerable region. Geophys. Res. Lett. 29 (11), 9–1.
- Steiner, A.L., Tonse, S., Cohen, R.C., Goldstein, A.H., Harley, R.A., 2006. Influence of future climate and emissions on regional air quality in California. J. Geophys. Res. Atmos. (1984–2012) 111 (D18).
- Tai, A.P., Mickley, L.J., Jacob, D.J., 2010. Correlations between fine particulate matter (PM 2.5) and meteorological variables in the United States: implications for the sensitivity of PM 2.5 to climate change. Atmos. Environ. 44 (32), 3976–3984.
- Val Martin, M., Heald, C.L., Lamarque, J.F., Tilmes, S., Emmons, L.K., Schichtel, B.A., 2015. How Emissions, Climate, and Land Use Change Will Impact Mid-century Air Quality over the United States: a Focus on Effects at National Parks.
- Verstraeten, W.W., Neu, J.L., Williams, J.E., Bowman, K.W., Worden, J.R., Boersma, K.F., 2015. Rapid increases in tropospheric ozone production and export from China. Nat. Geosci. 8 (9), 690–695.
- Vutukuru, S., Griffin, R.J., Dabdub, D., 2006. Simulation and analysis of secondary organic aerosol dynamics in the South Coast Air Basin of California. J. Geophys. Res. Atmos. 111 (D10).
- Zhao, Z., Chen, S.H., Kleeman, M.J., Tyree, M., Cayan, D., 2011a. The impact of climate change on air quality-related meteorological conditions in California. Part I: present time simulation analysis. J. Clim. 24 (13), 3344–3361.
- Zhao, Z., Chen, S.H., Kleeman, M.J., Mahmud, A., 2011b. The impact of climate change on air quality-related meteorological conditions in California. Part II: present versus future time simulation analysis. J. Clim. 24 (13), 3362–3376.